RICE UNIVERSITY

Smooth Subdivision for Mixed Volumetric Meshes

by

Jan Philipp Hakenberg

A Thesis Submitted
in Partial Fulfillment of the
Requirements for the Degree

Master of Science

Approved, Thesis Committee:

Joe Warren, Professor
Computer Science

Ron Goldman, Professor
Computer Science

Lydia Kavraki, Professor
Computer Science

Houston, Texas

August, 2004

Smooth Subdivision for Mixed Volumetric Meshes

Jan Philipp Hakenberg

Abstract

We derive stationary subdivision rules on bi-uniform volumetric grids consisting of pairwise combinations of tetrahedra, octahedra, triangular prisms and cubes. We refine the existing framework of quasi-interpolants so that weight stencils are obtained by algebraic manipulation. The joint spectral radius test proves that our combined schemes yield C^2 limit functions.

Furthermore, we present an algorithm to subdivide an unstructured mesh consisting of the basic shapes enumerated above. The subdivision rules are generalized, such that smoothness is preserved across all faces and the effort of implementing the scheme remains low.

Acknowledgment

I would like to thank Scott Schaefer for the fruitful discussions we had and for patiently teaching me the legal syntax in C_{++}. The idea to design a mixed volumetric scheme is due to Joe Warren, who has been a kind advisor and has tolerated my slightly off-topic, time-consuming explorations. The company SensAble Technologies provided us a haptic 3D input device, which was fun to design programs for. Ulrich Reif first introduced me to subdivision algorithms at the TU-Darmstadt. He initiated my acceptance to public support and pushed me to travel over-sea to work with his colleague Joe Warren.

Many people at Rice made my stay a very agreeable one – thank you all! I am also grateful to my family that supported me by keeping me up to date on what's going on at home.

Contents

Illustrations

Chapter 1

Introduction

Subdivision is a technique in computer aided geometric design for approximating a smooth surface by a sequence of increasingly faceted polyhedra. Subdivision schemes have several attributes that have motivated their development ever since the fundamental work of [CC78], [DS78] and [Lo87]: The input that a designer or artist provides to the algorithm, usually a coarse mesh, is manageable in size and the subdivision iteration on the mesh, determined by a simple set of affine combinations, typically results in a smooth surface. Today subdivision algorithms find their main application in industrial design and computer animations, for instance in modelling the skin of a humanoid character.

While a huge variety of subdivision algorithms exist to conveniently generate smooth surfaces, less attention has been given to volumetric subdivision schemes. In this thesis we derive stationary subdivision rules on bi-uniform volumetric meshes consisting of pairwise combinations of tetrahedra, octahedra, triangular prisms and cubes. We refine the existing framework of quasi-interpolants so that weight stencils can be computed by algebraic manipulation. The joint spectral radius test developed in [$L^2$03] proves that our combined schemes yield C^2 limit functions.

In the final chapter, the rules are generalized to almost arbitrary mesh configurations; nevertheless the effort of implementing the scheme remains low. In analogy to subdivision schemes for surfaces in 3D, the input to our volumetric subdivision algorithm is an unstructured mesh consisting of the basic shapes enumerated above. In one round of subdivision each shape is split into multiple smaller basic shapes, such that the result is again a 3D mesh. Several iterations of this process result in a

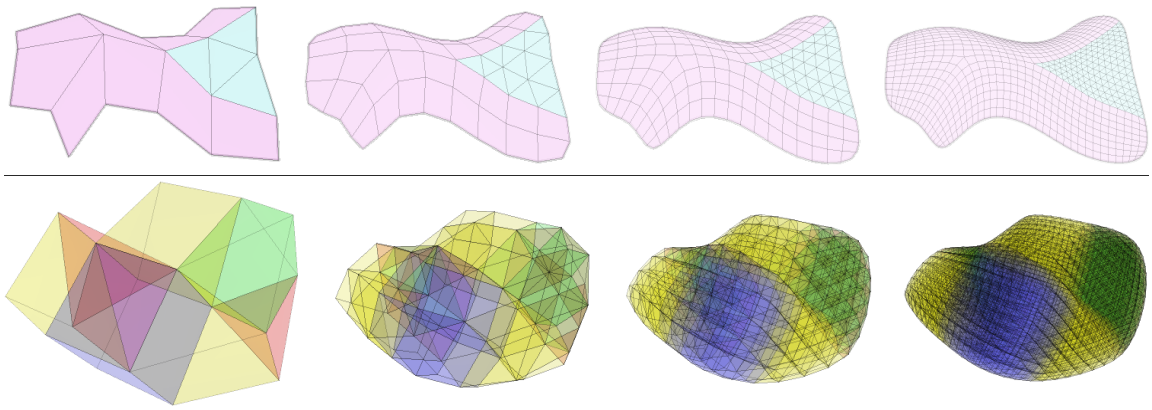

Figure 1.1 : Three rounds of subdivision of a surface mesh. Below, volumetric subdivision of a mesh consisting initially of 3 tetrahedra, 1 octahedron, 3 triangular prisms and 1 cube.

fine partitioning of space as illustrated in figure 1.1. For our generalized subdivision scheme we can guarantee smoothness everywhere except at extraordinary edges and vertices.

Our approach is motivated by the work on combined triangular-quad schemes in [$L^2$03] and [SW03]. Both papers discuss subdivision schemes that process meshes containing triangles and quads, which offers great freedom in surface modeling. Formerly, smooth subdivision algorithms were restricted to meshes consisting of either one of the polygon types. Our volumetric scheme is very similar in nature because we aim to develop a subdivision algorithm on mixed volumetric meshes containing tetrahedra, octahedra, triangular prisms and cubes. The theory for deriving the subdivision rules builds on the paper on polynomial generation and quasi-interpolation in stationary non-uniform subdivision [Le03].

Previous work on volumetric subdivision includes [BS02], which introduced subdivision rules for hexahedral meshes in the framework of factored subdivision. Averaging rules from 1- and 2-dimensions are generalized to higher dimensional hexahedral grids, including volume grids built out of cubes. The paper on smooth subdivi-

sion of tetrahedral meshes [SW04] explains how subdivision is performed on meshes consisting of tetrahedra and octahedra. We revisit and translate the scheme into a quasi-interpolant formulation.

The rules of the two afore mentioned volumetric subdivision schemes are preferable because the symmetry of the uniform grid is precisely reflected in the weights. In fact subdivision by our more general scheme does not differ from [BS02] when restricted to cubes, and does not differ from [SW04] when restricted to tetrahedra and octahedra.

Several other subdivision schemes on unstructured volume elements have been proposed in the past. [CJ96] presents a technique to subdivide 3D lattices of arbitrary topology, originally motivated by freeform deformation. However, the authors provide no smoothness analysis. Another subdivision method for tetrahedral meshes is proposed in [CD02]. The subdivision rules are related to box splines. Initially, diagonals are assigned to each tetrahedra, so that the split of each tetrahedron into 8 smaller tetrahedra is well determined. Distinct initial assignments lead to different subdivision outcomes. Again, no smoothness analysis is provided.

Volumetric subdivision has several applications. [CJ96] and [SW04] describe among others, how to deform a geometric model by embedding it into a coarse volumetric mesh, which is then subdivided and which controls the deformation. The principle is depicted in figure 1.2. The smoothness of the volumetric subdivision algorithm ensures that deformation happens gradually and does not produce creases on the surface of the model. In section 5.5 we illustrate how the variety of shapes that we provide helps to encapsulate the model in a manner reasonable for the desired deformations.

The fine partitioning of space generated by a volume mesh after a few rounds of volumetric subdivision can be used to build context related databases. In contrast to uniform or adaptive rectified space partitioning, the meshes considered by our new subdivision algorithm can be brought into almost exact alignment with boundary creases or other features of a volumetric region of interest. An example application is

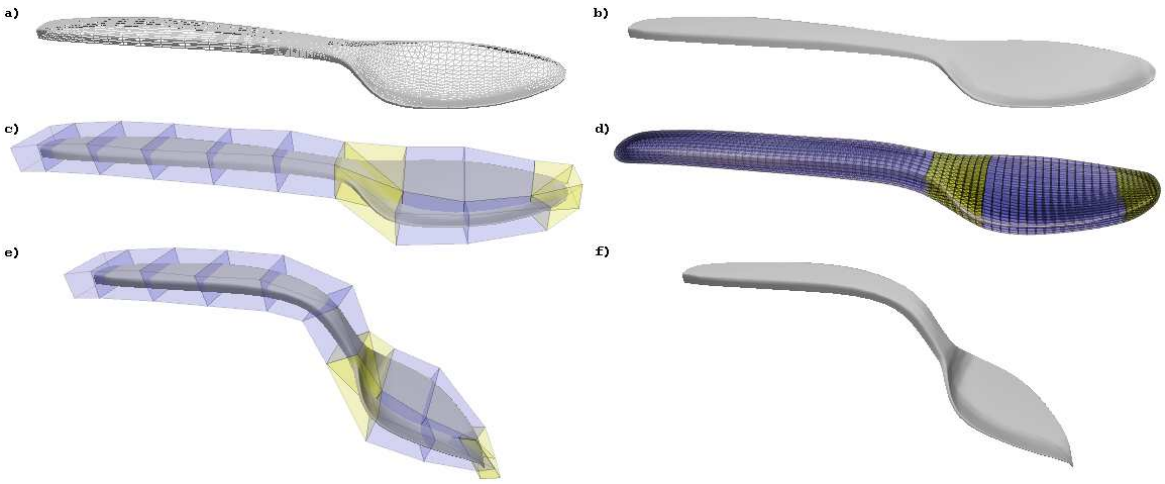

Figure 1.2 : a) shows wireframe of a spoon model, shaded in b). c) displays an embedding of the spoon in a volumetric control mesh. Barycentric coordinates of the vertices of the spoon are determined with respect to the shapes of the subdivided volume mesh in d). Modifying the vertices of the volumetric control mesh results in a deformation of the spoon.

the gene-expression database for the mouse brain viewable on `www.geneatlas.org`. A coarse volumetric mesh is defined so that several rounds of subdivision deliver a mesh almost perfectly aligned to the features and areas of the brain, and each tiny volumetric cell belongs entirely to one functional brain region. Since each cell is assigned information about local gene-expression, it is important that no two contextural distinct brain areas contribute to the same cell.

This thesis is structured in the following way: Chapters 2 and 3 discuss selected subdivision algorithms with emphasis on quasi-interpolant formulations. Chapter 4 contains the major theoretical contribution of this thesis, in that we derive how to combine two subdivision schemes along a common boundary into a smooth bi-uniform scheme. Also, we perform the relevant combinations that are of importance for our general algorithm. In Chapter 5, we present the volumetric subdivision algorithm on unstructured mixed meshes. The chapter is designed for a broad audience and knowledge from previous sections is not mandatory.

Chapter 2

Background

This chapter introduces notation, the reader might be unfamiliar with or which might appear ambiguous. We give the formal definition of uniform subdivision schemes. Since the framework of quasi-interpolants is particularly useful for combining two uniform stationary subdivision schemes along a common boundary, we also discuss the content of [Le03]. As examples, we visit the famous univariate cubic B-spline subdivision scheme, as well as the box-spline subdivision scheme on a regular triangular mesh.

2.1 Notation

Let $m \in \mathbb{N}$, $j = (j_1, j_2, ..., j_s) \in \mathbb{Z}^s$, $k \in \mathbb{Z}^s$ and $x, y \in \mathbb{R}^s$. Then in multi-index notation

$$|j| = |j_1| + |j_2| + ... + |j_s|$$
$$j \geq 0 \Longleftrightarrow j_1, j_2, ..., j_s \geq 0$$
$$j \equiv_m k \Longleftrightarrow j_i \equiv k_i \bmod m \quad \forall i \in \{1, ..., s\}$$
$$x^j = x_1^{j_1} x_2^{j_2} ... x_s^{j_s}.$$

For $j \geq 0$ we define $j! = j_1! j_2! \cdot ... \cdot j_s!$ and $D^j = \frac{\partial^{|j|}}{\partial^{j_1} x_1 \partial^{j_2} x_2 ... \partial^{j_s} x_s}$.

Let $\lambda \in \mathbb{R}$ and $A \in \mathbb{R}^{s \times s}$. For arithmetic operations on subsets of $\mathbb{R}^s \supset X$ we define

$$X + y = \{x + y \mid x \in X\}$$
$$\lambda X = \{\lambda x \mid x \in X\}$$
$$AX = \{Ax \mid x \in X\}.$$

A subset $X \subset \mathbb{R}^s$ is called symmetric if $x \in X \Longrightarrow -x \in X$.

Let $C^m(\mathbb{R}^s)$ denote the space of all m-times differentiable functions from $\mathbb{R}^s$ to $\mathbb{R}$ whose m-th order derivatives are continuous.

$$\nabla = (\frac{\partial}{\partial x_1}, \frac{\partial}{\partial x_2}, ..., \frac{\partial}{\partial x_s}) \qquad \text{and} \qquad \Delta = \frac{\partial^2}{\partial^2 x_1} + \frac{\partial^2}{\partial^2 x_2} + ... + \frac{\partial^2}{\partial^2 x_s}.$$

The function space of polynomials with degree $\leq m$ over the domain $X \subset \mathbb{R}^s$ is $\pi_m(X) = span\{f \mid f : X \longrightarrow \mathbb{R}, f(x) = x^i, 0 \leq |i| \leq m\}$. For the identity operator $Id\colon X \subset \mathbb{R}^s \longrightarrow \mathbb{R}^s$ we have $Id(x) = x$.

For a countable set X we denote the function space $l(X) = \{f \mid f\colon X \longrightarrow \mathbb{R}\}$. Whenever we write $f|_Y$ for $f \in l(X)$ and a finite subset $Y = \{y_1, ..., y_n\} \subset X$ we may use $f|_Y$ as a column vector with $f(y_i)$ as the i-th entry. Whenever we write $f|_X$ for a function $f\colon \mathbb{R}^s \longrightarrow \mathbb{R}$ and a countable, infinite set $X \subset \mathbb{R}^s$, then $f|_X$ is treated as an element of $l(X)$.

Furthermore, we use the sets

$$\mathbb{Z}^+ = \{1, 2, ...\} \qquad \mathbb{Z}_0^+ = \{0, 1, 2, ...\}$$

$$\mathbb{Z}^- = \{-1, -2, ...\} \qquad \mathbb{Z}_0^- = \{0, -1, -2, ...\}.$$

2.2 Uniform subdivision

A *uniform* subdivision operator is a linear operator $S : l(\mathbb{Z}^s) \longrightarrow l(\mathbb{Z}^s)$ defined by a finitely supported mask $a \in l(\mathbb{Z}^s)$ through

$$S(P)(\alpha) = \sum_{\beta \in \mathbb{Z}^s} a(\alpha - 2\beta)P(\beta).$$

For an arbitrary initial set of control points $P_0 \in l(\mathbb{Z}^s)$ a *stationary* subdivision scheme is defined by the iteration

$$P_n = SP_{n-1} = S^n P_0 \qquad \forall n \in \mathbb{Z}^+,$$

i.e. the operator S is invariant in the course of the iteration. The scheme S is called *uniformly convergent*, if for all $P_0 \in l(\mathbb{Z}^s)$, there is a continuous function $F : \mathbb{R}^s \longrightarrow \mathbb{R}$

with

$$\lim_{n\to\infty} \max_{z\in\mathbb{Z}^s\cap 2^n X} |S^n P_0(z) - F(2^{-n}z)| = 0,$$

for any open and bounded domain $X \subset \mathbb{R}^s$. In this case, we denote by $S^\infty P_0 = F$ the limit function of P_0 generated by subdivision. As part of the definition of *uniform convergence* we require that $S^\infty P_0$ is non-zero for some P_0.

For a uniformly convergent scheme S, the notion of a basis function $\Phi\colon \mathbb{R}^s \longrightarrow \mathbb{R}$ is captured by the definition

$$\Phi = S^\infty \delta \qquad \text{where} \qquad \delta \in l(\mathbb{Z}^s) \;\text{ is }\; \delta(z) = \begin{cases} 1 & z = 0 \\ 0 & \text{otherwise} \end{cases}.$$

Then $S^\infty P_0 = \sum_{\alpha\in\mathbb{Z}^s} P_0(\alpha)\Phi(\cdot - \alpha)$, and Φ satisfies the 2-scale relation

$$\Phi(\cdot) = \sum_{\alpha\in\mathbb{Z}^s} a(\alpha)\Phi(2\cdot - \alpha). \tag{2.2.1}$$

A scheme belongs to the *class* C^m, if the basis function $\Phi \in C^m(\mathbb{R}^s)$.

Every mask a can be aligned at the origin so that $\xi \in \mathbb{Z}_0^+$ is minimal in

$$a(\alpha) = 0 \qquad \forall \alpha \in \mathbb{Z}^s \setminus [-\xi, \xi]^s.$$

Then, $\Omega = [-\xi, \xi]^s$ is called the *support* of S.

The *weight stencil at* $\bar\lambda \in \mathbb{Z}^s$ is defined as $w_{\bar\lambda} \in l(\mathbb{Z}^s)$ with $w_{\bar\lambda}(\beta) = a(\bar\lambda - 2\beta)$. For a particular scheme there are essentially only 2^s different weight stencils up to translation. They can be considered representatives of the equivalence relation

$$w_{\bar\lambda_1} \sim w_{\bar\lambda_2} \Longleftrightarrow \bar\lambda_1 \equiv_2 \bar\lambda_2.$$

A weight stencil $w_{\bar\lambda}$ is supported in the *one-ring*, if $w_{\bar\lambda}(\beta) = 0$ for all $\beta \in \mathbb{Z}^s \cap ([-1, 1]^s - \frac{\bar\lambda}{2})$.

2.3 Quasi-Interpolants

[Le03] shows that every stationary uniformly convergent subdivision scheme satisfies

$$S^\infty(f|_{\mathbb{Z}^s}) = \sum_{|i|\le m} \frac{m_i}{i!} D^i f \qquad \forall f \in \pi_m(\mathbb{R}^s), \tag{2.3.1}$$

in which the moments m_i are given by

$$m_i = \sum_{\beta \in \mathbb{Z}^s} \Phi(-\beta)\beta^i. \tag{2.3.2}$$

When restricted to polynomial input, equation 2.3.1 expresses the operator $S^\infty : \pi_m(\mathbb{Z}^s) \longrightarrow \pi_m(\mathbb{R}^s)$ as a linear combination of differential operators. The operator $Q \colon \pi_m(\mathbb{R}^s) \longrightarrow \pi_m(\mathbb{Z}^s)$ that satisfies $S^\infty Q = Id$ is called the *quasi-interpolant* of the scheme S.

The operator $Q \colon \pi_m(\mathbb{R}^s) \longrightarrow l(X)$ for a countable unbounded set $X \subset \mathbb{R}^s$ is said to *preserve leading coefficients*, if

$$f \in \pi_k \Longrightarrow |Qf(x) - f(x)| = o(\|x\|^k), \qquad \text{as } \|x\| \longrightarrow \infty, x \in X.$$

for all $k \leq m$. For functions $f \colon \mathbb{R}^s \longrightarrow \mathbb{R}^s$ the dilation operater σ acts as $\sigma(f) = f(\frac{\cdot}{2})$.

In this context [Le03] proves the following

Corollary 2.1. *If S is convergent, S^∞ is injective, and $Q \colon \pi_m(\mathbb{R}^s) \longrightarrow l(X)$ preserves leading coefficients, then*

$$S^\infty Q = Id \iff SQ = Q\sigma, \tag{2.3.3}$$

both identities restricted to $\pi_m(\mathbb{R}^s)$.

In the case where S is unknown but the quasi-interpolant Q is fixed to a linear combination of derivatives that preserves leading coefficients over $X = \mathbb{Z}^s$, from the rhs in equivalence 2.3.3 we establish 2^s systems of linear equations, of which the solutions correspond to the weight stencil representatives in the mask a that determines S.

To solve for a single stencil $w_{\bar{\lambda}} \in l(\mathbb{Z}^s)$ at $\bar{\lambda} \in \mathbb{Z}^s$, we fix a finite support $\Lambda = \{\lambda_1, \lambda_2, ..., \lambda_n\} \subset \mathbb{Z}^s$, where $w_{\bar{\lambda}}$ is assumed to be zero outside of Λ. $w_{\bar{\lambda}}$ as a $|\Lambda|$-column vector is a solution of

$$M_{Q(\Lambda)} w_{\bar{\lambda}} = b_{Q(\bar{\lambda})} \tag{2.3.4}$$

where $M_{Q(\Lambda)}$ denotes a $\binom{m+s}{s} \times |\Lambda|$ matrix and b a $\binom{m+s}{s}$-column vector with entries

$$m_{ij} = Q(x^i)(\lambda_j) \qquad \text{and} \qquad b_i = Q(\frac{x^i}{2^{-|i|}})(\bar{\lambda})$$

with the multi-index $i \geq 0$, $0 \leq |i| \leq m$ and $j \in \{1, ..., |\Lambda|\}$. A solution satisfying 2.3.4 might not exist, in which case the quasi-interpolant Q and/or the stencil support Λ has to be altered.

Example 2.1. For the univariate cubic B-spline subdivision scheme the operator $S\colon l(\mathbb{Z}) \longrightarrow l(\mathbb{Z})$ is defined by the mask

$$a|_{[-2,2]} = \frac{1}{2}\frac{1}{2}[1 \;\; 2 \;\; 1] * \frac{1}{2}[1 \;\; 2 \;\; 1] = \frac{1}{8}[1 \;\; 4 \;\; 6 \;\; 4 \;\; 1], \tag{2.3.5}$$

and a is zero outside of the support $\Omega = [-2, 2]$. The scheme converges uniformly. The basis function $\Phi \in C^2(\mathbb{R})$ is a piecewise cubic polynomial. Repeated application of the operator S to the control point sequence P_0 interpreted on the narrowing diadic grid $2^{-n}\mathbb{Z}$ in the limit resembles the function $S^\infty P_0$. Two essential weight stencil representants are

$$w_0|_{[-1,1]} = \frac{1}{8}[1 \;\; 6 \;\; 1] \qquad \text{and} \qquad w_1|_{[0,1]} = \frac{1}{8}[4 \;\; 4].$$

Let $x^i\colon \mathbb{R} \longrightarrow \mathbb{R}$ be the monomial of degree i over $\mathbb{R}$. For the choice of $P_0 = x^i|_{\mathbb{Z}}$ as the sampling of the monomial over the integers, it can be shown that

$$\begin{aligned} S^\infty(x^0|_{\mathbb{Z}}) &\equiv 1 \\ S^\infty(x^1|_{\mathbb{Z}}) &= x \\ S^\infty(x^2|_{\mathbb{Z}}) &= x^2 + \tfrac{1}{3} \\ S^\infty(x^3|_{\mathbb{Z}}) &= x^3 + x \end{aligned} \tag{2.3.6}$$

The term $S^\infty(x^4|_{\mathbb{Z}})$ cannot be expressed as a linear combination of finitely many monomials over $\mathbb{R}$. Therefore we say that the scheme reproduces polynomials up to degree three. In [Le03] the four equations in 2.3.6 are combined into $S^\infty\colon \pi_3(\mathbb{Z}) \longrightarrow \pi_3(\mathbb{R})$ as

$$S^\infty(f|_{\mathbb{Z}}) = f + \frac{1}{6}\Delta f \qquad \forall f \in \pi^3(\mathbb{R}).$$

Due to the linearity of S^∞, we understand that

$$\begin{aligned} S^\infty(1|_{\mathbb{Z}}) &= x^0 \\ S^\infty(x|_{\mathbb{Z}}) &= x^1 \\ S^\infty((x^2 - \tfrac{1}{3})|_{\mathbb{Z}}) &= x^2 \\ S^\infty((x^3 - x)|_{\mathbb{Z}}) &= x^3, \end{aligned}$$

i.e. in order to generate a monomial x^i up to degree 3 as the result of B-spline subdivision, the quasi-interpolant $Q\colon \pi_3(\mathbb{R}) \longrightarrow \pi_3(\mathbb{Z})$ with

$$Q(f) = (f - \frac{1}{6}\Delta f)|_{\mathbb{Z}} \qquad \forall f \in \pi^3(\mathbb{R}) \tag{2.3.7}$$

maps x^i to the appropriate initial control points. Suppose a is unknown. Choose Q as in eq. 2.3.7. Then the weight stencil w_0 with support $\Lambda = \{-1, 0, 1\}$

$$M_{Q(\Lambda)} w_0|_\Lambda = \begin{pmatrix} 1 & 1 & 1 \\ -1 & 0 & 1 \\ \frac{2}{3} & -\frac{1}{3} & \frac{2}{3} \\ 0 & 0 & 0 \end{pmatrix} w_0|_\Lambda = \begin{pmatrix} 1 \\ 0 \\ -\frac{1}{12} \\ 0 \end{pmatrix} = b_{Q(0)}$$

has the unique solution $w_0|_\Lambda = \frac{1}{8}[1 \quad 6 \quad 1]$ and 0 outside of Λ. The computation is analogous for the remaining stencil w_1 with support $\Lambda' = \{0, 1\}$ by solving

$$M_{Q(\Lambda')} w_1|_{\Lambda'} = \begin{pmatrix} 1 & 1 \\ 0 & 1 \\ -\frac{1}{3} & \frac{2}{3} \\ 0 & 0 \end{pmatrix} w_1|_{\Lambda'} = \begin{pmatrix} 1 \\ \frac{1}{2} \\ \frac{1}{6} \\ 0 \end{pmatrix} = b_{Q(1)}$$

with the unique solution $w_1|_{\Lambda'} = \frac{1}{8}[4 \quad 4]$. Both stencils, w_0 and w_1, are supported in the one-ring.

Example 2.2. As another example we consider the box-spline subdivision scheme on a regular triangular mesh, whose generalization is the well-known Loop scheme.

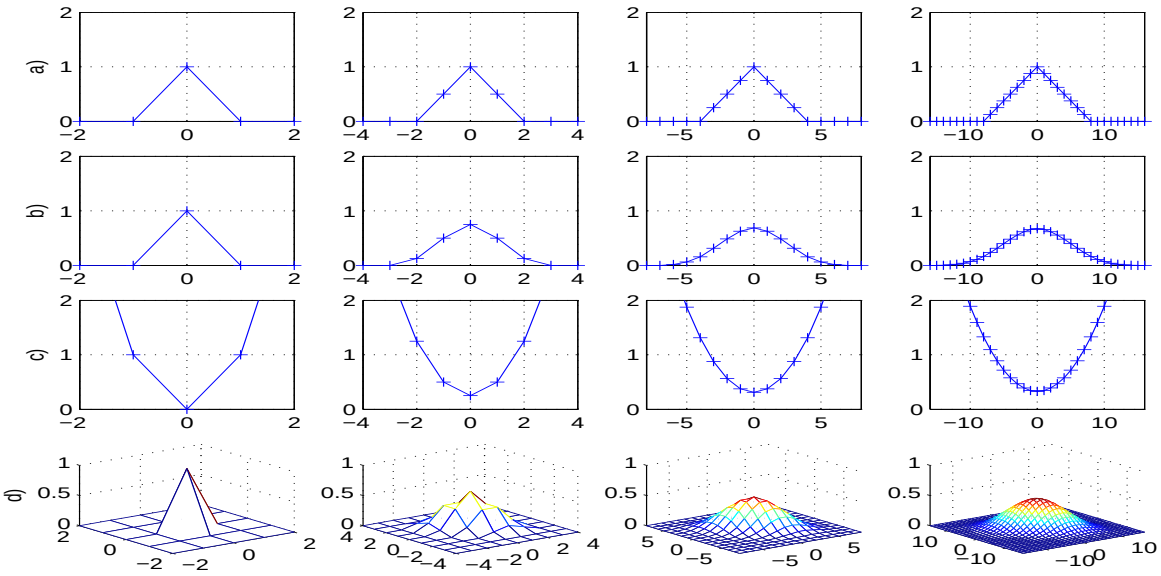

Figure 2.1 : Each row except c) represents three rounds of subdivision for the initial control point sequence $P_0 = \delta$, displayed over the non-zero part. The values are connected by lines to emphasize shape. a) shows subdivision via the mask $\frac{1}{2}[1 \;\; 2 \;\; 1]$. b) depicts δ, $S\delta$, $S^2\delta$ and $S^3\delta$ where S is from the cubic B-spline example 2.1, also in c) but with $P_0 = x^2|_{\mathbb{Z}}$ converging to $F = x^2 + \frac{1}{3}$. d) represents an approximation to $S^\infty\delta = \Phi$ the basis function of the scheme in example 2.2.

The subdivision operator is defined by the mask

$$a|_{[-2,2]^2} = \frac{1}{2^2}\frac{1}{2}\begin{bmatrix} 0 & 1 & 1 \\ 1 & 2 & 1 \\ 1 & 1 & 0 \end{bmatrix} * \frac{1}{2}\begin{bmatrix} 0 & 1 & 1 \\ 1 & 2 & 1 \\ 1 & 1 & 0 \end{bmatrix} = \frac{1}{16}\begin{bmatrix} 0 & 0 & 1 & 2 & 1 \\ 0 & 2 & 6 & 6 & 2 \\ 1 & 6 & 10 & 6 & 1 \\ 2 & 6 & 6 & 2 & 0 \\ 1 & 2 & 1 & 0 & 0 \end{bmatrix}. \tag{2.3.8}$$

[Le03] shows that the underlying operator $S^\infty \colon \pi_3(\mathbb{Z}^2) \longrightarrow \pi_3(\mathbb{R}^2)$ is of the form

$$S^\infty(f|_{\mathbb{Z}^2}) = f + \frac{1}{6}\nabla \begin{pmatrix} 1 & 1/2 \\ 1/2 & 1 \end{pmatrix} \nabla^T f$$

and the quasi-interpolant $Q \colon \pi_3(\mathbb{R}^2) \longrightarrow \pi_3(\mathbb{Z}^2)$ is

$$Q(f) = f|_{\mathbb{Z}^2} - \frac{1}{6}(\nabla \begin{pmatrix} 1 & 1/2 \\ 1/2 & 1 \end{pmatrix} \nabla^T f)|_{\mathbb{Z}^2},$$

The above representation for S^∞ is obtained by substituting the non-zero evaluations of the corresponding basis function $\Phi \colon \mathbb{R}^2 \longrightarrow \mathbb{R}$ at integer points, namely $\Phi(0,0) = \frac{1}{2}$ and

$$\Phi(1,0) = \Phi(0,1) = \Phi(1,1) = \Phi(-1,0) = \Phi(0,-1) = \Phi(-1,-1) = \frac{1}{12},$$

into expression 2.3.2 to yield the moments in equation 2.3.1 up to order 3 as

$$m_{(0,0)} = 1, \quad m_{(2,0)} = m_{(0,2)} = \frac{1}{3}, \quad m_{(1,1)} = \frac{1}{6}$$

while $m_i = 0$ for $i \in \mathbb{Z}^2$ with $i \geq 0$ and $|i| \in \{1, 3\}$.

2.4 Discrete convolution

Let the operator $V_{A,\nu} : l(A\mathbb{Z}^s) \longrightarrow l(A\mathbb{Z}^s)$ be defined by a finitely supported mask $\nu \in l(A\mathbb{Z}^s)$ and an invertible matrix $A \in \mathbb{R}^{s\times s}$ through

$$V_{A,\nu}(P)(\alpha) = \sum_{\beta \in A\mathbb{Z}^s} \nu(\alpha - \beta)P(\beta) \qquad \forall \alpha \in A\mathbb{Z}^s.$$

Then $V_{A,\nu}$ is called a *discrete convolution operator* on $A\mathbb{Z}^s$. On the particular grid $\mathbb{Z}^s$ the convolution operator is commonly abbreviated to $V_{I,\nu}(P) = \nu * P$ as in the equations 2.3.5 and 2.3.8.

We say for finite subsets of the grid $X, Y \subset A\mathbb{Z}^s$ X *computes* ν *on* Y, if there is a matrix $U \in \mathbb{R}^{|Y|\times|X|}$ such that

$$U(P|_X) = V_{A,\nu}(P)|_Y \qquad \forall P \in l(A\mathbb{Z}^s). \tag{2.4.1}$$

Finite differences are examples of discrete convolution operators. They approximate derivatives of a function sampled over a uniform grid. We present several masks ν of such operators according to our needs and without derivation. All operators are exact for polynomials of degree ≤ 3. The symbolic equation

$$\partial_{xx} \check{=} \nu|_{[-1,1]} = [1 \quad -2 \quad 1] \tag{2.4.2}$$

abbreviates $f''(z) = 1f(z-1) - 2f(z) + 1f(z+1)\ \forall z \in 1\mathbb{Z}$ for all univariate polynomials f up to degree 3 and ν is zero on the remaining domain $\mathbb{Z} \setminus [-1, 1]$. The discretized Laplace operator in the bivariate setting on the grid $\mathbb{Z}^2$ is expressed by the mask

$$\Delta = \partial_{xx} + \partial_{yy} \check{=} \nu|_{[-1,1]^2} = \begin{bmatrix} 0 & 1 & 0 \\ 1 & -4 & 1 \\ 0 & 1 & 0 \end{bmatrix}. \tag{2.4.3}$$

Also on the grid $\mathbb{Z}^2$ the mixed partial of second order is discretized by

$$\partial_{xy} \check{=} \nu|_{[-1,1]^2} = \begin{bmatrix} \frac{\zeta-1}{4} & \frac{-\zeta}{2} & \frac{\zeta+1}{4} \\ \frac{-\zeta}{2} & \zeta & \frac{-\zeta}{2} \\ \frac{\zeta+1}{4} & \frac{-\zeta}{2} & \frac{\zeta-1}{4} \end{bmatrix} \qquad \forall \zeta \in \mathbb{R}. \tag{2.4.4}$$

Not so common is the approximation of the derivatives of a function sampled over the grid $A\mathbb{Z}^2$, where $A = [e_1|\rho]$ with $e_1 = (1, 0)^T$ and $\rho = (-\frac{1}{2}, \frac{\sqrt{3}}{2})^T \in \mathbb{R}^2$. This grid is the natural choice for a parametrization over a triangular mesh and in this thesis we will make use of the following relations:

$$(\partial_{xx}+\partial_{yy})f \check{=} -4f(\cdot) + \frac{2}{3}[f(\cdot+e_1)+f(\cdot+\rho+e_1)+f(\cdot+\rho)+f(\cdot-e_1)+f(\cdot-\rho-e_1)+f(\cdot-\rho)] \tag{2.4.5}$$

which is the sum of the separate masks

$$\partial_{xx}\check{=}\nu|_\Theta = \begin{pmatrix} & 0 & 0 & \\ 1 & -2 & 1 \\ & 0 & 0 & \end{pmatrix} \qquad \text{and} \qquad \partial_{yy}\check{=}\nu|_\Theta = \begin{pmatrix} & \frac{2}{3} & \frac{2}{3} & \\ -\frac{1}{3} & -2 & -\frac{1}{3} \\ & \frac{2}{3} & \frac{2}{3} & \end{pmatrix}$$

where $\Theta = \{(0,0), e_1, e_1+\rho, \rho, -e_1, -e_1-\rho, -\rho\}$. The mixed partial of second order is discretized to

$$\partial_{xy}\check{=}\nu|_\Theta = \begin{pmatrix} -\frac{1}{\sqrt{3}} & \frac{1}{\sqrt{3}} \\ 0 & 0 & 0 \\ \frac{1}{\sqrt{3}} & -\frac{1}{\sqrt{3}} \end{pmatrix}.$$

Chapter 3

Uniform subdivision

So far, we have encountered univariate cubic B-spline subdivision and the bivariate box-spline scheme on triangles. This chapter revisits the tetrahedral-octahedral scheme of [SW04] and derives the corresponding quasi-interpolant.

We will construct triangular prism and cube subdivision schemes of class C^2 by the well known technique of tensoring subdivision schemes. The idea behind tensoring is to combine multiple low dimensional subdivision schemes into one higher dimensional scheme.

Furthermore, we show how the quasi-interpolant is modified when subdividing over the more general embedding $A\mathbb{Z}^s$, where A is an invertible matrix from $\mathbb{R}^{s\times s}$. In all the subdivision schemes of the thesis the corresponding quasi-interpolant transforms according to a simple algebraic formula. While leaving the weight stencils of the subdivision operator invariant, the modified quasi-interpolant maps each monomial up to a certain degree to the right set of control points, so that applying S^∞ returns the original monomial.

3.1 Cubic precision

In general, the support Ω of the subdivision mask a grows with smoothness demands on the limit functions or equivalently on the basis function Φ of a scheme. Large support introduces difficulties not only on the implementation of the scheme, but also on the extention of the rules to arbitrary meshes.

The case of polynomial reproduction up to degree $m = 3$ is of special interest because the subdivision weights are non-trivial only in the one-ring around a control

point while limit functions are usually of class C^2 in the uniform setting. From a practical point of view, one may also argue that visually appealing, smooth surfaces or meshes are generated. The mathematical tools in this chapter are all specialized for the reproduction of cubic polynomials, the setting where $m = 3$.

Lemma 3.1. *Let* $S^\infty \colon \pi_3(\mathbb{Z}^s) \longrightarrow \pi_3(\mathbb{R}^s)$ *and* $Q \colon \pi_3(\mathbb{R}^s) \longrightarrow \pi_3(\mathbb{Z}^s)$. *Then* $S^\infty Q = Id$ *implies*

$$S^\infty(f|_{\mathbb{Z}^s}) = f + \nabla H \nabla^T f \qquad \Longleftrightarrow \qquad Q(f) = f|_{\mathbb{Z}^s} - (\nabla H \nabla^T f)|_{\mathbb{Z}^s}$$

$\forall H \in \mathbb{R}^{s \times s}$.

Proof. By straight forward computation

$$\begin{aligned} S^\infty Q(f) &= S^\infty[f|_{\mathbb{Z}^s} - (\nabla H \nabla^T f)|_{\mathbb{Z}^s}] \\ &= S^\infty(f|_{\mathbb{Z}^s}) - S^\infty[(\nabla H \nabla^T f)|_{\mathbb{Z}^s}] \\ &= f + \nabla H \nabla^T f - \nabla H \nabla^T f + \sum_{0 \le j, |j|=4} \beta_j D^j f \end{aligned}$$

for appropriate factors $\beta_j \in \mathbb{R}$. Since with $0 \le j$, $|j| = 4$, $D^j f = 0 \quad \forall f \in \pi_3(\mathbb{R}^s)$ the bottom term simplifies to $S^\infty Q(f) = f$. □

We may abbreviate with a slight abuse of notation $S^\infty = Id + \nabla H \nabla^T$ and $Q = Id - \nabla H \nabla^T$.

Example 3.1. The tetrahedral-octahedral subdivision scheme from [SW04] is defined over $\mathbb{Z}^3$ by the mask $a = \frac{1}{2^3} m * m$ where $m \in l(\mathbb{Z}^3)$ with

$$m|_{[-1,1]^3} = \frac{1}{6} \left[\begin{array}{ccc|ccc|ccc} 0 & 0 & 1 & 0 & 3 & 3 & 1 & 3 & 1 \\ 0 & 3 & 3 & 3 & 6 & 3 & 3 & 3 & 0 \\ 1 & 3 & 1 & 3 & 3 & 0 & 1 & 0 & 0 \end{array}\right] \tag{3.1.1}$$

and m is zero everywhere else. We omit the display of a, which is expressed by a $5 \times 5 \times 5$ array with 85 non-zero entries. The support of S is $\Omega = [-2, 2]^3$, if the center element of the latter array is identified with $a(0)$.

The operator S^∞ follows from eq. 2.3.1, which involves the values of the basis function $\Phi : \mathbb{R}^s \longrightarrow \mathbb{R}$ at the integers. [Le03] notices that these correspond to the entries of the eigenvector to eigenvalue 1 of the matrix originating from the identity

$$\Phi(\beta) = \sum_{\alpha \in \Omega} a(\alpha)\Phi(2\beta - \alpha) \qquad \forall \beta \in \Omega,$$

which exploits the fact, that Φ is identically zero outside Ω. The eigenvector is scaled such that the entries sum up to 1. For the tetrahedral-octahedral scheme S the non-zero evaluations of Φ at the integers are in $[-1,1]^3 \subset \mathbb{Z}^3$ with

$$\Phi|_{[-1,1]^3} = \frac{1}{774} \left[\begin{array}{ccc|ccc|ccc} 0 & 0 & 5 & 0 & 38 & 38 & 5 & 38 & 5 \\ 0 & 38 & 38 & 38 & 288 & 38 & 38 & 38 & 0 \\ 5 & 38 & 5 & 38 & 38 & 0 & 5 & 0 & 0 \end{array}\right].$$

From eq. 2.3.2 we obtain all moments up to order 3 as

$$\begin{aligned} m_{(0,0,0)} &= 1 \\ m_{(2,0,0)} &= m_{(0,2,0)} = m_{(0,0,2)} = \tfrac{1}{3} \\ m_{(0,1,1)} &= m_{(1,0,1)} = m_{(1,1,0)} = -\tfrac{1}{9} \\ m_i &= 0 \qquad \text{for } |i| \in \{1,3\}. \end{aligned}$$

Substitution into eq. 2.3.1 yields $S^\infty \colon \pi_3(\mathbb{Z}^s) \longrightarrow \pi_3(\mathbb{R}^s)$ with

$$S^\infty(f|_{\mathbb{Z}^3}) = f + \nabla \begin{pmatrix} \frac{1}{6} & -\frac{1}{18} & -\frac{1}{18} \\ -\frac{1}{18} & \frac{1}{6} & -\frac{1}{18} \\ -\frac{1}{18} & -\frac{1}{18} & \frac{1}{6} \end{pmatrix} \nabla^T f$$

where the coefficients of the mixed partial derivatives are distributed symmetrically. According to lemma 3.1 the operator S^∞ differs from its inverse operator Q essentially only in the intermediate sign.

The author of the thesis seizes the opportunity to point out, that, although he is named a coauthor of the paper [SW04], he has really only contributed with a figure.

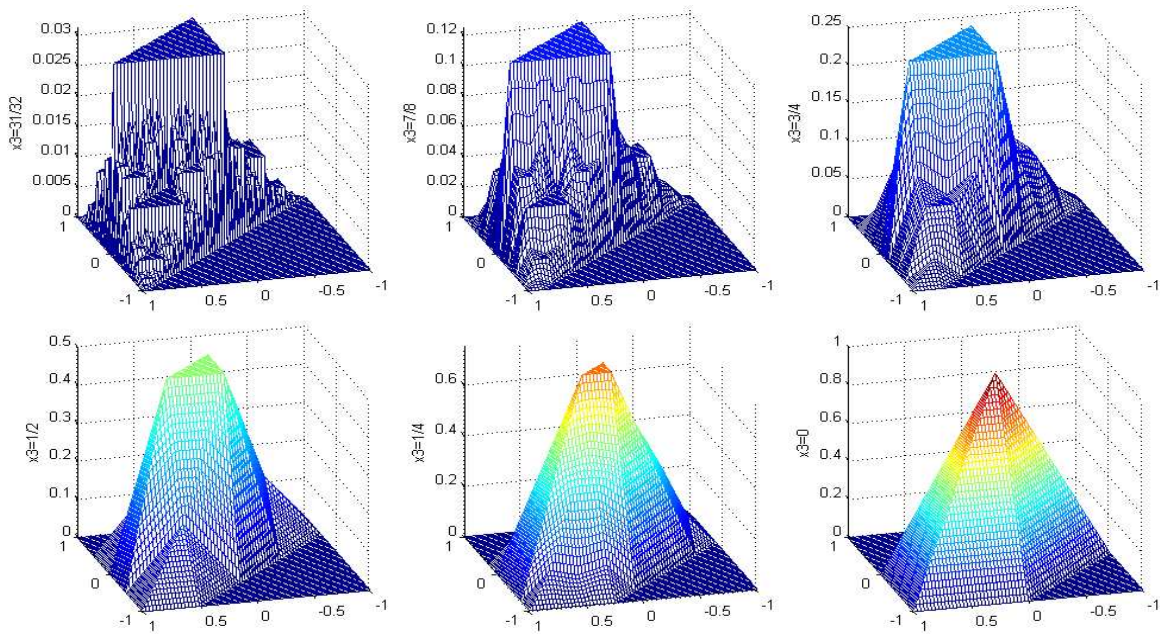

Figure 3.1 : Cross–sections of the continuous fractal basis function $\Phi_m : \mathbb{R}^3 \longrightarrow \mathbb{R}$ of the subdivision scheme defined by the mask m in expression 3.1.1. Display of the function $\Phi_m(\cdot, \cdot, x_3)$ for several fixed values of x_3, where the first two parameters range in the interval $[-1, 1]^2$. The height of each plot is individually scaled to enhance details. From the 2-scale relation in equation 2.2.1 and the identity $a = \frac{1}{2^3} m * m$ it follows that the basis function of the tetrahedral-octahedral scheme in example 3.1 satisfies $\Phi = \Phi_m * \Phi_m$.

3.2 Tensor product schemes

Definition 3.1. Let $S_1 : l(\mathbb{Z}^{s_1}) \longrightarrow l(\mathbb{Z}^{s_1})$ and $S_2 : l(\mathbb{Z}^{s_2}) \longrightarrow l(\mathbb{Z}^{s_2})$ be two subdivision operators with finitely supported masks $a_1 \in l(\mathbb{Z}^{s_1})$ and $a_2 \in l(\mathbb{Z}^{s_2})$. The tensor product subdivision operator $S = S_1 \otimes S_2$ is defined as $S : l(\mathbb{Z}^{s_1+s_2}) \longrightarrow l(\mathbb{Z}^{s_1+s_2})$ with

$$S(P)[(\alpha_1, \alpha_2)] = \sum_{\beta=(\beta_1,\beta_2)\in\mathbb{Z}^{s_1+s_2}} a_1(\alpha_1 - 2\beta_1)a_2(\alpha_2 - 2\beta_2)P(\beta) \tag{3.2.1}$$

for all $(\alpha_1, \alpha_2) \in \mathbb{Z}^{s_1+s_2}$.

One can show that if Φ_1 and Φ_2 are the basis functions of the schemes S_1 and S_2, then the basis function Φ of the tensored scheme $S = S_1 \otimes S_2$ satisfies

$$\Phi(\gamma) = \Phi_1(\gamma_1)\Phi_2(\gamma_2) \qquad \forall \gamma = (\gamma_1, \gamma_2) \in \mathbb{R}^{s_1+s_2}. \tag{3.2.2}$$

The moments m_i of S can be computed for each $i = (i_1, i_2) \in \mathbb{Z}^{s_1+s_2}$ as

$$\begin{aligned} m_{(i_1,i_2)} &= \sum_{(\beta_1,\beta_2)\in\mathbb{Z}^{s_1+s_2}} \Phi_1(-\beta_1)\Phi_2(-\beta_2)\beta_1^{i_1}\beta_2^{i_2} \\ &= \sum_{\beta_1\in\mathbb{Z}^{s_1}} \Phi_1(-\beta_1)\beta_1^{i_1} \sum_{\beta_2\in\mathbb{Z}^{s_2}} \Phi_2(-\beta_2)\beta_2^{i_2} = m_{1,i_1}m_{2,i_2} \end{aligned} \tag{3.2.3}$$

where $m_{k,i}$ denotes the i-th moment of scheme S_k for $k \in \{1, 2\}$.

The following lemma suits our purposes for constructing higher dimensional uniform subdivision schemes.

Lemma 3.2. *For two subdivision schemes $S_1^\infty : \pi_3(\mathbb{Z}^{s_1}) \longrightarrow \pi_3(\mathbb{R}^{s_1})$ and $S_2^\infty : \pi_3(\mathbb{Z}^{s_2}) \longrightarrow \pi_3(\mathbb{R}^{s_2})$ of the form $S_1^\infty(f|_{\mathbb{Z}^{s_1}}) = f + \nabla H_1 \nabla^T f$ and $S_2^\infty(f|_{\mathbb{Z}^{s_2}}) = f + \nabla H_2 \nabla^T f$, the operator $S^\infty : \pi_3(\mathbb{Z}^{s_1+s_2}) \longrightarrow \pi_3(\mathbb{R}^{s_1+s_2})$ of the tensored scheme $S = S_1 \otimes S_2$ satisfies*

$$S^\infty(f|_{\mathbb{Z}^{s_1+s_2}}) = f + \nabla \left(\begin{array}{c|c} H_1 & 0 \\ \hline 0 & H_2 \end{array}\right) \nabla^T f \qquad \forall f \in \pi_3(\mathbb{R}^{s_1+s_2}). \tag{3.2.4}$$

Proof. As part of the assumption we derive from eq. 2.3.1 that for $k \in \{1, 2\}$ the moments $m_{k,i}$ up to order 3 vanish whenever $|i| \in \{1, 3\}$.

According to eqs. 2.3.1 and 3.2.3 we compute $m_0 = m_{1,0}m_{2,0} = 1$. Now let $i = (i_1, i_2) \in \mathbb{Z}^{s_1+s_2}$ be $|i| \geq 1$. For $|i| = 1$ we can deduce that w.l.o.g. $|i_1| = 1$ and $|i_2| = 0$, so $m_i = m_{1,i_1}m_{2,i_2} = 0 \cdot 1 = 0$. For moments m_i with $|i| = 2$ we destinguish between three cases:

1) $|i_1| = 2$ and $|i_2| = 0$ so that $m_i = m_{1,i_1}m_{2,i_2} = m_{1,i_1}$. Hence, these 2-nd order moments can be taken from H_1.

2) $|i_1| = 0$ and $|i_2| = 2$ is similar to 1), except that the moments now coincide with the entries of H_2.

3) $|i_1| = 1$ and $|i_2| = 1$ so that $m_i = m_{1,i_1}m_{2,i_2} = 0 \cdot 0 = 0$, which correspond to the entries trivially zero in the matrix of eq. 3.2.4.

For $|i| = 3$ we have w.l.o.g $|i_1| \in \{1, 3\}$. Hence $m_{1,i_1} = 0$, which cancels the product with m_{2,i_2}. □

With a view towards volumetric subdivision we give

Example 3.2. Tensoring the univariate cubic B-spline scheme S_1 from example 2.1 with the box-spline scheme S_2 from example 2.2 yields a subdivision scheme for a uniform triangular prism grid. Using lemma 3.2, we derive for $S = S_1 \otimes S_2$

$$S^\infty(f|_{\mathbb{Z}^3}) = f + \nabla \left(\begin{array}{c|cc} \frac{1}{6} & 0 & 0 \\ \hline 0 & \frac{1}{6} & \frac{1}{12} \\ 0 & \frac{1}{12} & \frac{1}{6} \end{array}\right) \nabla^T f \qquad \forall f \in \pi_3(\mathbb{R}^s). \tag{3.2.5}$$

Example 3.3. We construct the subdivision scheme for an s-dimensional cube mesh by tensoring the univariate cubic B-spline scheme S_1 in the manner $S = \underbrace{S_1 \otimes ... \otimes S_1}_{s}$. Repeated application of lemma 3.2 yields

$$S^\infty(f|_{\mathbb{Z}^s}) = f + \nabla \left(\begin{array}{cc|c} \frac{1}{6} & 0 & 0 \\ 0 & \ddots & 0 \\ \hline 0 & 0 & \frac{1}{6} \end{array}\right) \nabla^T f \qquad \forall f \in \pi_3(\mathbb{R}^s)$$

or simply $S^\infty = Id + \frac{1}{6}\Delta$. Note that uniform subdivision on quads over the grid $\mathbb{Z}^2$ and on cubes over $\mathbb{Z}^3$ corresponds to the cases $s = 2$ and $s = 3$.

3.3 Grid transformation

For a particular subdivision scheme the grid $\mathbb{Z}^s$ is not always considered the canonic embedding. For instance for the scheme on triangles from example 2.2 we intuitively consider the set

$$\begin{pmatrix} 1 & -\frac{1}{2} \\ 0 & \frac{\sqrt{3}}{2} \end{pmatrix} \mathbb{Z}^2 = \left\{ (z_1 - \frac{1}{2}z_2, \frac{\sqrt{3}}{2}z_2) | (z_1, z_2) \in \mathbb{Z}^2 \right\}$$

the natural grid embedding, depicted also in figure 4.7.b. In the transformed configuration the symmetries of each weight stencil at a point $\bar{\lambda}$ of the triangular grid coincide with the grid symmetries around $\frac{\bar{\lambda}}{2}$.

We postpone the definition of subdivision over uniform grids of the form $A\mathbb{Z}^s$ where A has full rank to the next chapter. But in the context of uniform subdivision we give

Definition 3.2. For a quasi-interpolant $Q : \pi_m(\mathbb{R}^s) \longrightarrow \pi_m(\mathbb{Z}^s)$ and a matrix $A \in \mathbb{R}^{s\times s}$ we define the operator

$$Q_A : \pi_m(\mathbb{R}^s) \longrightarrow \pi_m(A\mathbb{Z}^s)$$

$$Q_A(f)(Az) = Q(f \circ \varphi)(z) \qquad \forall f \in \pi_m(\mathbb{R}^s), z \in \mathbb{Z}^s$$

with $\varphi : \mathbb{R}^s \longrightarrow \mathbb{R}^s$ and $\varphi(x) = Ax$.

Application of the chain rule delivers

Lemma 3.3. *Let $Q : \pi_3(\mathbb{R}^s) \longrightarrow \pi_3(\mathbb{Z}^s)$ be of the form $Q(f) = f|_{\mathbb{Z}^s} - (\nabla H \nabla^T f)|_{\mathbb{Z}^s}$ with $H \in \mathbb{R}^{s\times s}$. Then the operator Q_A is of the form*

$$Q_A(f) = f|_{A\mathbb{Z}^s} - (\nabla A H A^T \nabla^T f)|_{A\mathbb{Z}^s}$$

Proof. Again, let $\varphi : \mathbb{R}^s \longrightarrow \mathbb{R}^s$ with $\varphi(x) = Ax$. Then $\nabla\varphi = A$ and

$$\begin{aligned} Q_A(f)(Az) &= Q(f \circ \varphi)(z) \\ &= (f \circ \varphi)(z) - (\nabla H \nabla^T (f \circ \varphi))(z) \\ &= f(Az) - \nabla[HA^T(\nabla^T f) \circ \varphi](z) \\ &= f(Az) - (\nabla AHA^T \nabla^T f \circ \varphi)(z) \\ &= f(Az) - (\nabla AHA^T \nabla^T f)(Az). \end{aligned}$$

□

Example 3.4. Consider the quasi-interpolant of the C^2 subdivison scheme on a uniform triangular mesh presented in example 2.2 with $Q = Id - \nabla H \nabla^T$ where

$$H = \begin{pmatrix} \frac{1}{6} & \frac{1}{12} \\ \frac{1}{12} & \frac{1}{6} \end{pmatrix}.$$

For the grid transformation defined by the matrix

$$A = \begin{pmatrix} 1 & -\frac{1}{2} \\ 0 & \frac{\sqrt{3}}{2} \end{pmatrix}$$

according to previous lemma the quasi-interpolant $Q_A : \pi_3(\mathbb{R}^2) \longrightarrow \pi_3(A\mathbb{Z}^2)$ adapts as

$$\begin{aligned} Q_A(f) &= f|_{A\mathbb{Z}^2} - (\nabla \begin{pmatrix} 1 & -\frac{1}{2} \\ 0 & \frac{\sqrt{3}}{2} \end{pmatrix} \begin{pmatrix} \frac{1}{6} & \frac{1}{12} \\ \frac{1}{12} & \frac{1}{6} \end{pmatrix} \begin{pmatrix} 1 & 0 \\ -\frac{1}{2} & \frac{\sqrt{3}}{2} \end{pmatrix} \nabla^T f)|_{A\mathbb{Z}^2} \\ &= f|_{A\mathbb{Z}^2} - \frac{1}{8}(\nabla\nabla^T f)|_{A\mathbb{Z}^2} \end{aligned}$$

or simply $Q_A = Id - \frac{1}{8}\Delta$.

Example 3.5. Consider the tetrahedral-octahedral scheme from example 3.1. Under the linear grid transformation with

$$A = \begin{pmatrix} 1 & \frac{1}{2} & \frac{1}{2} \\ 0 & \frac{\sqrt{3}}{2} & \frac{1}{2\sqrt{3}} \\ 0 & 0 & \sqrt{\frac{2}{3}} \end{pmatrix} \quad \text{and recalling that} \quad H = \begin{pmatrix} \frac{1}{6} & -\frac{1}{18} & -\frac{1}{18} \\ -\frac{1}{18} & \frac{1}{6} & -\frac{1}{18} \\ -\frac{1}{18} & -\frac{1}{18} & \frac{1}{6} \end{pmatrix}$$

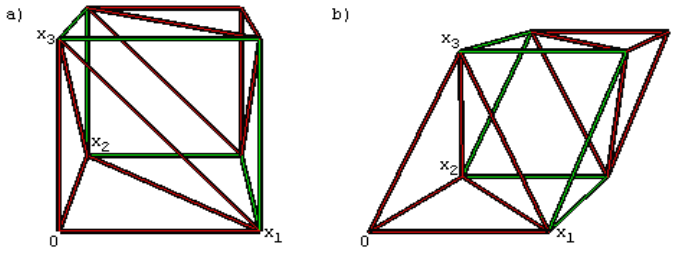

Figure 3.2 : a) displays the embedding of the tetrahedral-octahedral scheme over $\mathbb{Z}^3$ in the interval $[0,1]^3$. b) shows transformed tetrahedral-octahedral grid in $A[0,1]^3$. Edges induced by the subdivision weights are added to the graphs. In b) all edges are of the same Euclidean length. x_i for $i \in \{1,2,3\}$ label the grid spanning vectors.

the quasi-interpolant $Q_A \colon \pi_3(\mathbb{R}^3) \longrightarrow \pi_3(A\mathbb{Z}^3)$ is found as

$$Q_A(f) = f|_{A\mathbb{Z}^3} - (\nabla A H A^T \nabla^T f)|_{A\mathbb{Z}^3} = f|_{A\mathbb{Z}^3} - \frac{1}{9}(\Delta f)|_{A\mathbb{Z}^3},$$

which we may simplify to $Q_A = Id - \frac{1}{9}\Delta$. The subdivision weights in the mask a of the scheme feature the same symmetries as the tetrahedral-octahedral grid $A\mathbb{Z}^3$ in figure 3.2.b.

Chapter 4

Bi-uniform subdivision

First, we give a definition of bi-uniform subdivision, which provides the framework for combining two possibly distinct subdivision schemes along a common boundary. In this context, we review existing work on combining triangular-subdivision with quad-subdivision into a bi-uniform C^2 scheme.

We develop tools that simplify the weight stencil computations in the boundary region of a bi-uniform grid. When combining two volumetric subdivision schemes, we overcome the need to solve systems of linear equations, which would be fairly inconvenient to set up for stencils in three dimensions. Instead, the derivation of the rules for pairwise combinations of volumetric schemes, such as subdivision on tetrahedra/octahedra, triangular prisms and cubes, reduces to algebraic formula manipulation.

[$L^2$03] develop a technique to analyse the smoothness of a bi-uniform scheme. The technique is referred to as the *joint spectral radius test*, which is carried out by a computer. We apply the test to each of our newly derived schemes to prove that all combined schemes produce C^2 limit functions over $\mathbb{R}^3$.

4.1 Bi-uniform subdivision

The following framework is a specialization of the more general definition of *non-uniform* subdivision in [$L^2$03].

Definition 4.1. Let two invertible matrices $A, B \in \mathbb{R}^{s\times s}$ with $s \geq 2$ satisfy $A_{sj} = B_{sj} = 0$ for all $j \in \{1, ..., s-1\}$, $A_{ss}, B_{ss} > 0$ and $A_{1:s-1,1:s-1}\mathbb{Z}^{s-1} = B_{1:s-1,1:s-1}\mathbb{Z}^{s-1}$.

Then the *bi-uniform* grid spanned by A and B is defined as

$$g(A,B) = A(\mathbb{Z}^{s-1} \times \mathbb{Z}_0^-) \bigcup B(\mathbb{Z}^{s-1} \times \mathbb{Z}_0^+).$$

This definition ensures that the grid is uniform in each half-space, $x_s > 0$ and $x_s < 0$, and that the two grid halfs spanned by A and B are aligned to share a common $(s-1)$-dimensional boundary $A(\mathbb{Z}^{s-1} \times \{0\}) = B(\mathbb{Z}^{s-1} \times \{0\})$.

Subdivision operators on bi-uniform grids are linear operators with $S\colon l(g(A,B)) \longrightarrow l(g(A,B))$ defined by $2c+1$ finitely supported masks $a_{-c}, ..., a_0, ..., a_c \in l(\mathbb{Z}^s)$ for some $c \in \mathbb{Z}_0^+$ combined in

$$S(P)(\psi\alpha) = \sum_{\beta \in \mathbb{Z}^s} a_{\phi(\alpha_s)}(\alpha - 2\beta) P(\psi\beta) \qquad \forall \alpha \in \mathbb{Z}^s \tag{4.1.1}$$

where $\psi\colon \mathbb{Z}^s \longrightarrow g(A,B)$ with

$$\psi(\alpha) = \begin{cases} A\alpha & \alpha_s \leq 0 \\ B\alpha & \alpha_s > 0 \end{cases}$$

and $\phi\colon \mathbb{Z} \longrightarrow \{-c, ..., c\}$ defined by $\phi(i) = \min[\max(-c, \lfloor \frac{i}{2} \rfloor), c]$. Instead of listing the $2c+1$ masks, it is common to refer to the weight stencils, i.e. the extracts of each masks evaluated at every second entry, and to visualize how to obtain the sum in formula 4.1.1 graphically over the grid $g(A,B)$.

Repeated application of the same operator S to an initial set of control points $P_0 \in l(g(A,B))$ is characteristic for stationary subdivision schemes.

Since the set $2^{-n}g(A,B)$ for $n \longrightarrow \infty$ converges to a dense subset in $\mathbb{R}^s$, S is said to be *convergent*, if for all initial sets of control points $P_0 \in l(g(A,B))$ there exists a continuous function $F\colon \mathbb{R}^s \longrightarrow \mathbb{R}$ such that

$$\lim_{n \to \infty} \max_{x \in g(A,B) \cap 2^n X} |S^n P_0(x) - F(2^{-n}x)| = 0$$

for any open and bounded domain $X \subset \mathbb{R}^s$ and if $S^\infty P_0 \not\equiv 0$ for some $P_0 \in l(g(A,B))$. The scheme is of class C^m, if $F \in C^m(\mathbb{R}^s)$ for all possible P_0.

[$L^2$03] shows that if S can generate limit functions throughout π_m the space of polynomials of degree $\leq m$, then the existence of an inverse Q of S^∞ on π_m is implied. Conversely, if the operator S is unknown, subdivision weights can be obtained from a careful design of the quasi-interpolant operator $Q\colon \pi_3(\mathbb{R}^s) \longrightarrow l(g(A,B))$ because corrolary 2.1 applies also for $X = g(A,B)$.

The types of quasi-interpolant on $g(A,B)$ considered throughout this thesis are of the form

$$Q(f)(x) = \begin{cases} Q_A^-(f)(x) & x_s < 0 \\ \hat{Q}(f)(x) & x_s = 0 \\ Q_B^+(f)(x) & x_s > 0 \end{cases} \qquad x \in g(A,B)$$

where $Q^-\colon \pi_3(\mathbb{R}^s) \longrightarrow \pi_3(\mathbb{Z}^s)$ is from the uniform scenario with

$$Q^-(f) = (Id - \nabla H^- \nabla^T)(f)|_{\mathbb{Z}^s}$$

so that $Q_A^-\colon \pi_3(\mathbb{R}^s) \longrightarrow \pi_3(A(\mathbb{Z}^{s-1} \times \mathbb{Z}^-))$ modifies according to lemma 3.3 to

$$Q_A^-(f) = (Id - \nabla A H^- A^T \nabla^T)(f)|_{A(\mathbb{Z}^{s-1}\times\mathbb{Z}^-)}.$$

We denote $H_A = AH^-A^T$. Similarly, we define Q^+ and Q_B^+ so that $H_B = BH^+B^T$. The operator for the boundary $\hat{Q}\colon \pi_3(\mathbb{R}^s) \longrightarrow \pi_3(A(\mathbb{Z}^{s-1} \times \{0\}))$ is defined separately so that $\hat{Q}$ preserves leading coefficients.

To eliminate the redundancy in notation, we simply write $Q_A = Q_A^-$ and $Q_B = Q_B^+$ and define the global quasi-interpolant over a bi-uniform grid by stating each of the three operators in

$$Q(f)(x) = \begin{cases} Q_A(f)(x) & x_s < 0 \\ \hat{Q}(f)(x) & x_s = 0 \\ Q_B(f)(x) & x_s > 0 \end{cases} \qquad x \in g(A,B). \tag{4.1.2}$$

The transformations of Q_A and Q_B ensure that weight stencils from the univariate setting are preserved at points away from the boundary. Weight stencils whose support contains points from the boundary are called extraordinary; their computation is the central focus of this chapter.

In expression 4.1.2 three possibly distinct quasi-interpolants, Q_A, $\hat{Q}$ and Q_B, determine the evaluation of Q over $g(A,B)$. In general, the support $\Lambda \in g(A,B)$ for a weight stencil at $\bar{\lambda}$ might involve k different quasi-interpolants, in which case we partition the designated stencil support into the respective k pairwise disjoint sets Λ_l for $l = 1...k$. W.l.o.g. let $\bar{\lambda}$ be in the domain of Q_1. In analogy with the uniform setting [Le03] deduces a system of linear equations to solve for the weight stencil $\omega_{\bar{\lambda}}$ at $\bar{\lambda}$ from the rhs in eq. 2.3.3. The equations are of the form

$$M_{Q_1(\Lambda_1),...,Q_k(\Lambda_k)}\omega_{\bar{\lambda}} = [M_{Q_1(\Lambda_1)} \mid ... \mid M_{Q_k(\Lambda_k)}]\omega_{\bar{\lambda}} = b_{Q_1(\bar{\lambda})}, \tag{4.1.3}$$

which simply denotes a concatenation of matrices where each $M_{Q_l(\Lambda_l)}$ is a $\binom{m+s}{s} \times |\Lambda_l|$ matrix and b a $\binom{m+s}{s}$-column vector with entries

$$m_{ij} = Q_l(x^i)(\lambda_j) \qquad b_i = Q_1(\frac{x^i}{2^{-|i|}})(\bar{\lambda})$$

where the multi-index $i \geq 0$, $0 \leq |i| \leq m$ and $j \in \{1, ..., |\Lambda_l|\}$.

All the mathematical tools established in this chapter deal with eq. 4.1.3, solutions of which represent a weight stencil for a combined subdivision scheme. Note also, that the computation of the stencils in the uniform setting, originally introduced by equation 2.3.4, is a special case of the above identity.

Later in the chapter, we explain why, due to the invariance of the grid points $g(A,B)$ under translation by the $s-1$ first column vectors in A (interchangeable by B) along the boundary, the relation $2g(A,B) \subset g(A,B)$ and the grid uniformity away from the boundary, finitely many different weight stencils are obtained from expression 4.1.3 to describe a bi-uniform subdivision scheme.

Example 4.1. Both triangular-quad subdivision schemes of [$L^2$03] and [SW03] operate on the bi-uniform grid $g(A,B)$ spanned by

$$A = \begin{pmatrix} 1 & 0 \\ 0 & 1 \end{pmatrix} \qquad \text{and} \qquad B = \begin{pmatrix} 1 & -\frac{1}{2} \\ 0 & 1 \end{pmatrix}.$$

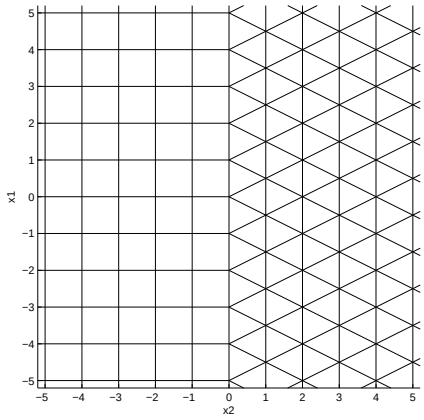

Figure 4.1 : Part of the bi-uniform triangular-quad grid. Edges are displayed as induced by subdivision weights.

The embedding combines triangles and quads along a common boundary as displayed in figure 4.1. The quasi-interpolant for uniform quads subdivision was presented in the scope of example 3.3. Since A is the identity matrix, no essential transformation occurs and we simply take

$$Q_A(f) = (Id - \nabla \begin{pmatrix} \frac{1}{6} & 0 \\ 0 & \frac{1}{6} \end{pmatrix} \nabla^T)(f)|_{\mathbb{Z}\times\mathbb{Z}^-}. \tag{4.1.4}$$

For the triangular side, i.e. where $x_2 > 0$, the quasi-interpolant from example 2.2 is properly transformed to

$$Q_B(f) = (Id - \nabla \begin{pmatrix} \frac{1}{8} & 0 \\ 0 & \frac{1}{6} \end{pmatrix} \nabla^T)(f)|_{B(\mathbb{Z}\times\mathbb{Z}^+)}. \tag{4.1.5}$$

As mentioned before, this transformation assures that ordinary subdivision rules apply at points whose stencil support does not include boundary elements.

For the definition of the quasi-interpolant on the boundary, [$L^2$03] prefers Q_A over Q_B in the sense that $\hat{Q}\colon \pi_3(\mathbb{R}^2) \longrightarrow \pi_3(A(\mathbb{Z}\times\{0\}))$ is chosen to be

$$\hat{Q}(f) = (Id - \nabla \begin{pmatrix} \frac{1}{6} & 0 \\ 0 & \frac{1}{6} \end{pmatrix} \nabla^T)(f)|_{\mathbb{Z}\times\{0\}}, \tag{4.1.6}$$

whereas the authors of [SW03] decide to average the matrices H_A and H_B in

$$\hat{Q}(f) = (Id - \nabla \begin{pmatrix} \frac{7}{48} & 0 \\ 0 & \frac{1}{6} \end{pmatrix} \nabla^T)(f)|_{\mathbb{Z}\times\{0\}}. \tag{4.1.7}$$

Note that in either case $\hat{Q}$ is chosen as a convex combination of the symbolical form

$$\hat{Q}_\mu = \mu Q_A + (1-\mu)Q_B$$

where $\mu = 1$ corresponds $\hat{Q}$ in eq. 4.1.6 and $\mu = \frac{1}{2}$ to eq. 4.1.7. Both versions produce limit functions in C^2 over $\mathbb{R}^2$, which was proved by applying the joint spectral radius test. Therefore we write $S^\infty P_0 \in C^2(\mathbb{R}^2)$ for all input $P_0 \in l(g(A,B))$.

The system of linear equation to solve for the stencil at $(0,0)$ for $\mu = \frac{1}{2}$ can be found in equation 4.3.12 the solution of which is visualized to emphasize the geometric context in the lhs of figure 4.4. The stencil support is the one-ring of $(0,0)$ consisting of the points

$$\Lambda = \left\{(1,-1),(0,-1),(-1,-1),(1,0),(0,0),(-1,0),(\frac{1}{2},1),(-\frac{1}{2},1)\right\} \subset g(A,B).$$

4.2 Close to the boundary

Whenever the quasi-interpolant on the boundary $\hat{Q}$ is distinct from the quasi-interpolant of a side of the bi-uniform grid and the ordinary stencil support contains points from the boundary, weights x have to be adjusted simply because the system of linear equations in 4.1.3 differs from the formula of the uniform setting 2.3.4. Also, the stencil support is likely to be extended, an example of which is given in figure 4.2. For reasonable and big enough support, the linear systems of equations in the more general expression 4.1.3 might provide a solution for such an extraordinary stencil. This section deals with how exactly for an existing stencil the support needs to be extended so that we can ensure a solution for a weight stencil whose ordinary support touches but does not overlap the boundary and hence needs to be modified. Under certain conditions the weights are adjusted according to a simple formula.

Lemma 4.1. *Let $\Lambda \subset g(A,B)$ be the support for the stencil at $\bar{\lambda} \in g(A,B)$ so that $M_{Q(\Lambda)}x = b_{Q(\bar{\lambda})}$ has a solution, and let $Q\hat{S}^{\infty} : \pi_m(A(\mathbb{Z}^{s-1} \times \{0\})) \longrightarrow \pi_m(A(\mathbb{Z}^{s-1} \times \{0\}))$ be expressable as a convolution operator with finitely supported mask ν and $\hat{\Lambda}$ computes ν on $\hat{\Lambda} \cap \Lambda$ exact for polynomials up to degree m. Then*

$$M_{Q(\Lambda\setminus\hat{\Lambda}),\hat{Q}(\hat{\Lambda})}\tilde{x} = b_{Q(\bar{\lambda})} \tag{4.2.1}$$

has a solution.

Proof. We constuct a matrix $Z \in \mathbb{R}^{|\Lambda\cup\hat{\Lambda}|\times|\Lambda|}$ with

$$M_{Q(\Lambda\setminus\hat{\Lambda}),\hat{Q}(\hat{\Lambda})}Z = [M_{Q(\Lambda\setminus\hat{\Lambda})} \mid M_{\hat{Q}(\hat{\Lambda})}]Z = M_{Q(\Lambda)}. \tag{4.2.2}$$

W.l.o.g. we partition $M_{Q(\Lambda)}$ as follows

$$M_{Q(\Lambda)} = [M_{Q(\Lambda\setminus\hat{\Lambda})} \mid M_{Q(\Lambda\cap\hat{\Lambda})}].$$

In view of the matrix multiplication the construction reduces to determining a rectangular matrix U with

$$[M_{Q(\Lambda\setminus\hat{\Lambda})} \mid M_{\hat{Q}(\hat{\Lambda})}] \cdot \left(\begin{array}{c|c} I & 0 \\ \hline 0 & U \end{array}\right) = [M_{Q(\Lambda\setminus\hat{\Lambda})} \mid M_{Q(\Lambda\cap\hat{\Lambda})}]. \tag{4.2.3}$$

Z takes over without modification the first columns $M_{Q(\Lambda\setminus\hat{\Lambda})}$ that are, by construction, identical to the first columns of $M_{Q(\Lambda)}$.

The convolution operator $Q\hat{S}^{\infty}$ with the mask ν has the effect that $Q\hat{S}^{\infty}\hat{Q}f = Qf$ for all polynomials f up to degree m. Since $\hat{\Lambda}$ computes ν on $\Lambda \cap \hat{\Lambda}$, we compute the matrix U from eq. 2.4.1. Each row of $M_{\hat{Q}(\hat{\Lambda})}$, represented by $\hat{Q}(f)|_{\hat{\Lambda}}^{T}$ for a monomial f, multiplied with U yields exact values of $Q(f)|_{\Lambda\cap\hat{\Lambda}}$ that generate the corresponding column of $M_{Q(\Lambda\cap\hat{\Lambda})}$.

With the matrix Z in hand, the system of linear equations in eq. 4.2.1 has a solution due to the identity 4.2.2 and the assumption that $M_{Q(\Lambda)}x = b_{Q(\bar{\lambda})}$ has a solution x. □

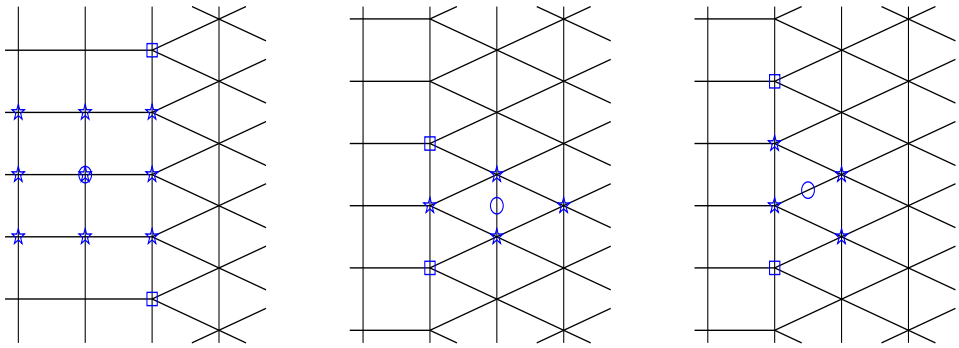

Figure 4.2 : Selected weight stencils close to the boundary. Stars indicate ordinary support. Control points marked by squares need to be joined to the support so that equation 4.2.1 has a solution.

Remark 4.1. The lemma with the constructive proof describes how one round of subdivision at $\bar{\lambda}$ might be factorizable into convolution followed by subdividing with weights x and support Λ from the uniform setting. Factorization is more apparent by writing

$$x^T Z^T (P|_{\Lambda \cup \hat{\Lambda}}) = \tilde{x}^T (P|_{\Lambda \cup \hat{\Lambda}}) \tag{4.2.4}$$

to determine $(SP)(\bar{\lambda})$, the value at grid point $\bar{\lambda}$, by one round of subdivision encountering only the values of $P \in l(g(A,B))$ at $\Lambda \cup \hat{\Lambda}$.

Example 4.2. We revisit the triangular-quad scheme from example 4.1, in particular the choice for $\hat{Q}$ in equation 4.1.7. Using lemma 4.1, we derive the subdivision rules for selected weight stencils whose support touches the boundary, as motivated by figure 4.2.

If the choice of the boundary quasi-interpolant $\hat{Q}$ is equal to the quasi-interpolant on the triangular side given in eq. 4.1.5

$$Q_B f = (Id - \nabla \begin{pmatrix} \frac{1}{8} & 0 \\ 0 & \frac{1}{6} \end{pmatrix} \nabla^T)(f)|_{g(A,B)},$$

weight stencils at grid points $\bar{\lambda}$ with $\bar{\lambda}_s > 0$ could be taken from the uniform triangular

scheme with the one-ring of $\bar{\lambda}$ as support. In other words, the solutions to

$$M_{Q_B(\Lambda)}x = b_{Q_B(\bar{\lambda})}$$

are known to exist for certain supports Λ depending on $\bar{\lambda}$.

The choice for the boundary operator $\hat{Q}$ in equation 4.1.7 differs from Q_B. When resticted to polynomials we determine the inverse of $\hat{Q}$ by lemma 3.3 to be $\hat{S}^\infty : \pi_3(\mathbb{Z}\times\{0\}) \longrightarrow \pi_3(\mathbb{R}\times\{0\})$ with

$$\hat{S}^\infty(f|_{\mathbb{Z}\times\{0\}}) = (Id + \nabla \begin{pmatrix} \frac{7}{48} & 0 \\ 0 & \frac{1}{6} \end{pmatrix} \nabla^T) f.$$

Through lemma 4.1 we find that the operator $Q_B\hat{S}^\infty : \pi_3(\mathbb{Z}\times\{0\}) \longrightarrow \pi_3(\mathbb{Z}\times\{0\})$ plays a crucial role in the weight stencil modification as soon as the support contains grid points from the boundary. For all polynomials f over $\mathbb{R}^2$ with degree ≤ 3

$$\begin{aligned} Q_B\hat{S}^\infty(f|_{\mathbb{Z}\times\{0\}}) &= (Id - \nabla \begin{pmatrix} \frac{1}{8} & 0 \\ 0 & \frac{1}{6} \end{pmatrix} \nabla^T)(Id + \nabla \begin{pmatrix} \frac{7}{48} & 0 \\ 0 & \frac{1}{6} \end{pmatrix} \nabla^T)(f)|_{\mathbb{Z}\times\{0\}} \\ &= (Id + \nabla \begin{pmatrix} \frac{1}{48} & 0 \\ 0 & 0 \end{pmatrix} \nabla^T)(f)|_{\mathbb{Z}\times\{0\}}. \end{aligned}$$

The operator $Q_B\hat{S}^\infty$ is expressed as a discrete convolution operator on the boundary $\mathbb{Z}\times\{0\}$ with the mask

$$\nu_B|_{[-1,1]} = [0 \;\; 1 \;\; 0] + \frac{1}{48}[1 \;\; -2 \;\; 1] = [\frac{1}{48} \;\; \frac{23}{24} \;\; \frac{1}{48}].$$

Similarly, one shows that $Q_A\hat{S}^\infty$ is equivalent to the convolution operator defined by the mask

$$\nu_A|_{[-1,1]} = [0 \;\; 1 \;\; 0] + \frac{-1}{48}[1 \;\; -2 \;\; 1] = [\frac{-1}{48} \;\; \frac{25}{24} \;\; \frac{-1}{48}].$$

We proceed using the notation of lemma 4.1. Let $\Lambda \subset g(A,B)$ be the ordinary stencil support touching, but not overlapping, the boundary. Then the set of grid points $\Lambda_0 = \Lambda \cap \mathbb{Z}\times\{0\}$ is the non-empty part of the ordinary support on the boundary, as illustrated in figure 4.2. The choice of $\hat{\Lambda}$ as the one-environment of Λ_0

$$\hat{\Lambda} = \left\{\xi \mid \xi \in g(A,B), \xi_s = 0, \exists\lambda \in \Lambda_0 \text{ with } \left\|A^{-1}(\xi-\lambda)\right\|_1 \leq 1\right\}$$

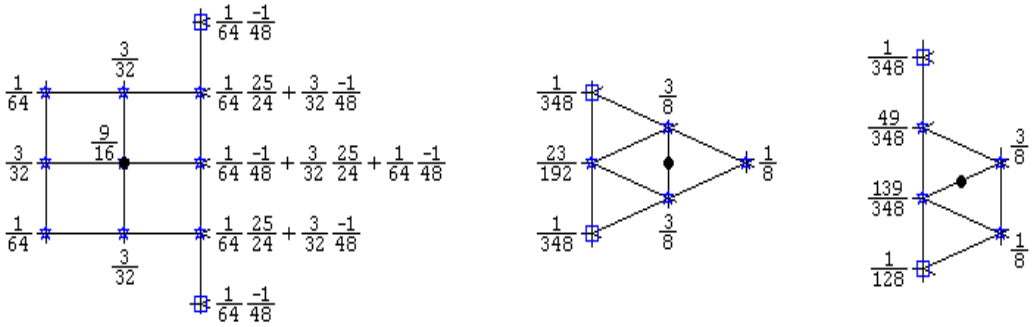

Figure 4.3 : The application of the convolution operators defined by the masks ν_A and ν_B to the boundary control points followed by ordinary subdivision on each side as derived in example 4.2.

restricted to the boundary is sufficient to compute ν_A on $\Lambda \cap \hat{\Lambda}$, due to the size of the support of ν_A. The same construction holds for ν_B. The ordinary weights are factored as is eq. 4.2.4, for instance as

$$\frac{1}{8}[1 \quad 3 \quad 3 \mid 1] \cdot \left(\begin{array}{c|cc} I & 0 & \\ \hline 0 & \frac{1}{48} & \frac{23}{24} \quad \frac{1}{48} \end{array}\right) = [\frac{1}{8} \quad \frac{3}{8} \quad \frac{3}{8} \quad \frac{1}{384} \quad \frac{23}{192} \quad \frac{1}{384}],$$

the rhs of which is the solution to a linear system of equations of the form $M_{Q_B(\Lambda\setminus\hat{\Lambda}),\hat{Q}(\hat{\Lambda})}\tilde{x} = b_{Q_B(\bar{\lambda})}$. Another example on the triangular side is

$$\frac{1}{8}[1 \quad 3 \mid 3 \quad 1] \cdot \left(\begin{array}{c|ccc} I & 0 & & \\ \hline & \frac{1}{48} & \frac{23}{24} \quad \frac{1}{48} & 0 \\ 0 & 0 & \frac{1}{48} \quad \frac{23}{24} & \frac{1}{48} \end{array}\right) = [\frac{1}{8} \quad \frac{3}{8} \quad \frac{1}{128} \quad \frac{139}{348} \quad \frac{49}{348} \quad \frac{1}{384}].$$

Figure 4.3 displays the newly derived weight stencils.

Remark 4.2. Since the masks ν_A and ν_B are applied to all control points along the boundary, one round of subdivision can be designed in the following way. First all the control points on the boundary are convolved with ν_A and ν_B. Because the masks are distinct, the control points on the boundary get duplicated. Ordinary subdivision rules then apply to the respective result of convolution, to yield the final control points away from the boundary.

In [SW03] the factorization is called *unzipping* followed by subdivision. The pair (ν_A, ν_B) is referred to as the *unzipping masks*.

4.3 On the boundary

Under certain conditions the intermediate quasi-interpolant $\hat{Q}$ can be chosen, so that a weight stencil at any point $\bar{\lambda}$ on the boundary of a bi-uniform grid can be constructed by the mean of two uniform weight stencils as illustrated in figure 4.4. As a consequence, the extraordinary stencils closely resemble the two uniform weight stencils, which is exploited in the implementation of the scheme.

In view of the next lemma we give

Definition 4.2. The half-sided moment to the non-negative multi-index $p \in \mathbb{Z}^s$ for the weight stencil representative to $i \in \mathbb{Z}^s/2\mathbb{Z}^s$ of a uniform subdivision scheme with finitely supported symmetric mask $a \in l(\mathbb{Z}^s)$ over the grid $A\mathbb{Z}^s$ spanned by an invertible matrix A is defined as

$$\varpi_{p,i} = \sum_{z \in \mathbb{Z}^{s-1} \times \mathbb{Z}_0^+} (1 - \frac{1}{2}\delta_{0,z_s}) a(i - 2z)[A(z - i/2)]^p$$

where δ is the Kronecker Delta. The order of the half-sided moment is $|p|$.

There are $\binom{s}{|p|}$ half sided moments of order $|p|$.

Example 4.3. Recall the triangular-quad subdivision from example 4.1. For the uniform quad scheme, with the identity as the grid generating matrix, the half-sided moments of first order for the stencil representatives to $(0,0)$ and $(1,0)$ are

$$\begin{aligned}
\varpi_{|1|,(0,0)} &= \tfrac{1}{2}\tfrac{3}{32}\begin{pmatrix} 1 \\ 0 \end{pmatrix} + \tfrac{1}{2}\tfrac{9}{16}\begin{pmatrix} 0 \\ 0 \end{pmatrix} + \tfrac{1}{2}\tfrac{3}{32}\begin{pmatrix} -1 \\ 0 \end{pmatrix} + \tfrac{1}{64}\begin{pmatrix} 1 \\ 1 \end{pmatrix} + \tfrac{3}{32}\begin{pmatrix} 0 \\ 1 \end{pmatrix} + \tfrac{1}{64}\begin{pmatrix} -1 \\ 1 \end{pmatrix} &&= \begin{pmatrix} 0 \\ \frac{1}{8} \end{pmatrix} \\
\varpi_{|1|,(1,0)} &= \tfrac{1}{2}\tfrac{3}{8}\begin{pmatrix} \frac{1}{2} \\ 0 \end{pmatrix} + \tfrac{1}{2}\tfrac{3}{8}\begin{pmatrix} -\frac{1}{2} \\ 0 \end{pmatrix} + \tfrac{1}{16}\begin{pmatrix} \frac{1}{2} \\ 1 \end{pmatrix} + \tfrac{1}{16}\begin{pmatrix} -\frac{1}{2} \\ 1 \end{pmatrix} &&= \begin{pmatrix} 0 \\ \frac{1}{8} \end{pmatrix}.
\end{aligned}$$

To achieve a better overview, we obtain the half-sided moments simultaneously. In the notation of the definition we write

$$\varpi_{(1,0),(0,0)} = 0, \quad \varpi_{(0,1),(0,0)} = \tfrac{1}{8}, \quad \varpi_{(1,0),(1,0)} = 0, \quad \varpi_{(0,1),(1,0)} = \tfrac{1}{8}.$$

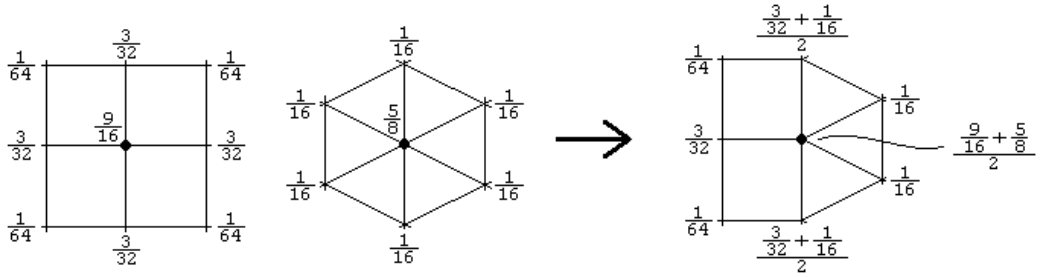

Figure 4.4 : Averaging the weights for a selected stencil on the triangular-quad boundary.

For the triangular scheme on the grid spanned by $B = \begin{pmatrix} 1 & -\frac{1}{2} \\ 0 & 1 \end{pmatrix}$,

$$\varpi'_{|1|,(0,0)} = \tfrac{1}{2}\ \tfrac{1}{16}\begin{pmatrix} 1 \\ 0 \end{pmatrix} + \tfrac{1}{2}\ \tfrac{5}{8}\begin{pmatrix} 0 \\ 0 \end{pmatrix} + \tfrac{1}{2}\ \tfrac{1}{16}\begin{pmatrix} -1 \\ 0 \end{pmatrix} + \tfrac{1}{16}\begin{pmatrix} \frac{1}{2} \\ 1 \end{pmatrix} + \tfrac{1}{16}\begin{pmatrix} -\frac{1}{2} \\ 1 \end{pmatrix} = \begin{pmatrix} 0 \\ \frac{1}{8} \end{pmatrix}$$

$$\varpi'_{|1|,(1,0)} = \tfrac{1}{2}\ \tfrac{3}{8}\begin{pmatrix} \frac{1}{2} \\ 0 \end{pmatrix} + \tfrac{1}{2}\ \tfrac{3}{8}\begin{pmatrix} -\frac{1}{2} \\ 0 \end{pmatrix} + \tfrac{1}{8}\begin{pmatrix} 0 \\ 1 \end{pmatrix} = \begin{pmatrix} 0 \\ \frac{1}{8} \end{pmatrix}$$

That the half sided moments match as $\varpi_{|1|,i} = \varpi'_{|1|,i}$ for the representants $i = (0,0)$ and $i = (1,0)$, i.e. stencils at boundary points, is not coincidence. In fact, the half sided moments of order 3 match as well.

Let $\Lambda \subset A\mathbb{Z}^s$ denote the support for a weight stencil. We use the following abbreviations to partition Λ:

$$\begin{aligned} \Lambda^- &= \Lambda \cap A(\mathbb{Z}^{s-1} \times \mathbb{Z}^-) \\ \Lambda^0 &= \Lambda \cap A(\mathbb{Z}^{s-1} \times \{0\}) \\ \Lambda^+ &= \Lambda \cap A(\mathbb{Z}^{s-1} \times \mathbb{Z}^+). \end{aligned}$$

Lemma 4.2. *Let $Q : \pi_2(\mathbb{R}^s) \longrightarrow l(g(A,B))$ be defined as in 4.1.2 as a combination of the uniform operators $Q_A(f) = (Id - \nabla H_A \nabla^T)(f)|_{A\mathbb{Z}^s}$ and $Q_B(f) = (Id - \nabla H_A \nabla^T)(f)|_{B\mathbb{Z}^s}$ away from the boundary. Let the half-sided moments of order 1 of the two uniform schemes match. Then solutions to*

$$M_{Q_A(\Lambda_A)} x_A = b_{Q_A(0)} \qquad \textit{and} \qquad M_{Q_B(\Lambda_B)} x_B = b_{Q_B(0)} \tag{4.3.1}$$

with symmetric supports Λ_A and Λ_B imply a solution of

$$M_{Q_A(\Lambda_A^-),\frac{1}{2}(Q_A+Q_B)(\Lambda_A^0\cup\Lambda_B^0),Q_B(\Lambda_B^+)}x = b_{\frac{1}{2}(Q_A+Q_B)(0)}. \tag{4.3.2}$$

Proof. Over the course of the proof it becomes clear that x_A and x_B can be transformed into symmetric solutions to eqs. 4.3.1, i.e. $x_A(\lambda) = x_A(-\lambda)$ for $\lambda \in \Lambda_A$ and analogous for x_B. For simplicity, we assume x_A and x_B are given symmetrically.

Monomials of even degree are even functions, whereas monomials of odd degree are odd functions over $\mathbb{R}^s$. The property of even or odd of a monomial is preserved by the operator Q_A in the sense that

$$\begin{aligned} Q_A(f)(Az) &= Q_A(f)(-Az) \quad \text{for even } f \in \pi_n(\mathbb{R}^s) \\ Q_A(f)(Az) &= -Q_A(f)(-Az) \quad \text{for odd } f \in \pi_n(\mathbb{R}^s) \end{aligned}$$

for all $z \in \mathbb{Z}^s$. Due to the symmetry of the support Λ_A, each control point location $\lambda \in \Lambda_A$ appears also as $-\lambda \in \Lambda_A$. We partition the product in eq. 4.3.1 as

$$M_{Q_A(\Lambda_A)}x_A = [\ M_{Q_A(\Lambda_A^-)} \mid M_{Q_A(\Lambda_A^0)} \mid M_{Q_A(\Lambda_A^+)}\ ] \cdot [\ x_A^- \mid x_A^0 \mid x_A^+\ ]. \tag{4.3.3}$$

Recall from equation 4.1.3 that each monomial f of degree ≤ 2 evaluated by the operator Q_A over the support Λ_A generates a row in $M_{Q_A(\Lambda_A)}$. Thus for the even monomials (those of degree 0 and 2) the rows in the matrices $M_{Q_A(\Lambda_A^-)}$ and $M_{Q_A(\Lambda_A^+)}$ can be column-permuted to be identical. For all linear monomials the operator Q_A acts like the identity and overall we can assure equality for

$$[\ M_{Q_A(\Lambda_A^-)} \mid M_{Q_A(\Lambda_A^0)}\ ] \cdot [\ x_A^- \mid \frac{1}{2}x_A^0\ ] = \bar{b}_A \tag{4.3.4}$$

where $\bar{b}_A$ has the entries of $\frac{1}{2}b_{Q_A(0)}$ for row entries corresponding to even monomials. The definition of the half-sided moment $\varpi_{e_i,0}$, where e_i is the i-th unit vector, coincides with the negative of the result by the matrix product in 4.3.4 at the entry of $\bar{b}_A$ that corresponds to the i-th linear monomial. Hence, we define $\bar{b}_A$ at that entry as $-\varpi_{e_i,0}$.

The same considerations hold for Q_B except that the split is carried out in favor of the positive support

$$[\ M_{Q_B(\Lambda_B^0)} \mid M_{Q_B(\Lambda_B^+)}\ ] \cdot [\ \frac{1}{2}x_B^0 \mid x_B^+\ ] = \bar{b}_B \tag{4.3.5}$$

in which $\bar{b}_B$ is constructed analogous to $\bar{b}_A$ in the sense that we insert $\frac{1}{2}b_{Q_B(0)}$ for row entries corresponding to even monomials and the positive half-sided moment $\varpi_{|1|,0}$ at the entries corresponding to the linear monomials.

By concatenation and addition of eqs. 4.3.4 and 4.3.5

$$[\, M_{Q_A(\Lambda_A^-)} \mid M_{Q_A(\Lambda_A^0)} \mid M_{Q_B(\Lambda_B^0)} \mid M_{Q_B(\Lambda_B^+)} \,] \cdot [\, x_A^- \mid \frac{1}{2}x_A^0 \mid \frac{1}{2}x_B^0 \mid x_B^- \,] = \bar{b}_A + \bar{b}_B \quad (4.3.6)$$

of which the excerpt from the center satisfies

$$[M_{Q_A(\Lambda_A^0)} \mid M_{Q_B(\Lambda_B^0)} \,] \cdot [\frac{1}{2}x_A^0 \mid \frac{1}{2}x_B^0 \,] = M_{\frac{1}{2}(Q_A+Q_B)(\Lambda_A^0 \cup \Lambda_B^0)} x^0 \quad (4.3.7)$$

for the vector

$$x^0 = \begin{cases} \frac{1}{2}x_A^0(\lambda) & \lambda \in \Lambda_A^0 \setminus \Lambda_B^0 \\ \frac{1}{2}[x_A^0(\lambda) + x_B^0(\lambda)] & \lambda \in \Lambda_A^0 \cap \Lambda_B^0 \\ \frac{1}{2}x_B^0(\lambda) & \lambda \in \Lambda_B^0 \setminus \Lambda_A^0 \end{cases} . \quad (4.3.8)$$

The entries of $\bar{b}_A + \bar{b}_B$ on the rhs of eqs. 4.3.6 corresponding to the linear monomials cancel and the resulting vector equals $b_{\frac{1}{2}(Q_A+Q_B)(0)}$. Hence from eqs. 4.3.6 and 4.3.7 we construct the system of linear equations in term 4.3.2 to

$$M_{Q_A(\Lambda_A^-), \frac{1}{2}(Q_A+Q_B)(\Lambda_A^0 \cup \Lambda_B^0), Q_B(\Lambda_B^+)} \begin{pmatrix} x_A^- \\ x^0 \\ x_B^+ \end{pmatrix} = b_{\frac{1}{2}(Q_A+Q_B)(0)} .$$

□

Note that the system of linear equations in 4.3.2 corresponds to the choice of $\hat{Q} = \frac{1}{2}(Q_A + Q_B)$ on the boundary. One can show, under similar conditions, a solution is generated in general for any $\hat{Q} = (1-\mu)Q_A + \mu Q_B$.

Remark 4.3. The lemma deals only with stencils at the origin. We are of course concerned with stencils throughout the boundary. [Le03] shows that solutions to

$$M_{Q_A(\Lambda_A)} x_A = b_{Q_A(\bar{\lambda})} \qquad \text{and} \qquad M_{Q_B(\Lambda_B)} x_B = b_{Q_B(\bar{\lambda})}$$

can alternatively be obtained from

$$M_{Q_A(\Lambda_A-\frac{\bar{\lambda}}{2})}x_A = b_{Q_A(0)} \qquad \text{and} \qquad M_{Q_B(\Lambda_B-\frac{\bar{\lambda}}{2})}x_B = b_{Q_B(0)} \tag{4.3.9}$$

whenever Q_A and Q_B are linear combinations of differential operators. Similarly, one derives that the solution space of

$$M_{Q_A(\Lambda_A^-),\frac{1}{2}(Q_A+Q_B)(\Lambda_A^0\cup\Lambda_B^0),Q_B(\Lambda_B^+)}x = b_{\frac{1}{2}(Q_A+Q_B)(\bar{\lambda})} \tag{4.3.10}$$

is equivalent to

$$M_{Q_A(\Lambda_A^--\frac{\bar{\lambda}}{2}),\frac{1}{2}(Q_A+Q_B)(\Lambda_A^0\cup\Lambda_B^0-\frac{\bar{\lambda}}{2}),Q_B(\Lambda_B^+-\frac{\bar{\lambda}}{2})}x = b_{\frac{1}{2}(Q_A+Q_B)(0)}, \tag{4.3.11}$$

for all weight stencils at a general boundary location $\bar{\lambda} \in g(A,B)$ where $\bar{\lambda}_s = 0$. The translation of the respective supports by $-\frac{\bar{\lambda}}{2}$ leaves the set Λ_A^- in the domain of Q_A, the set $\Lambda_A^0 \cup \Lambda_B^0$ in the domain of $\hat{Q}$ and Λ_B^+ in the domain of Q_B.

If the supports Λ_A and Λ_B of the stencils at $\bar{\lambda} \in A\mathbb{Z}^s$ of the uniform schemes on $A\mathbb{Z}^s$ and $B\mathbb{Z}^s$ are symmetric when translated by $-\frac{\bar{\lambda}}{2}$, lemma 4.2 applies to eqs. 4.3.11. Instead of inserting the half-sided moment $\varpi_{|1|,0}$, the columns corresponding to the linear monomials in $\bar{b}_A$ and $\bar{b}_B$ are assigned $\varpi_{|1|,i}$ where $i \equiv_2 z$ with $i \in \{0,1\}^s$.

The latter modification requires that in order to combine two subdivision schemes on $g(A,B)$, all $2^{|s-1|}$ half-sided moments of order one to the boundary stencil representants of the two transformed uniform schemes are identical.

Furthermore, we understand that a bi-uniform subdivision scheme is described by finitely many weight stencils, due to the translational invariance of the solutions of the equations 4.3.10 and 4.3.11.

Example 4.4. In the following we derive the weight stencil representative at (0,0) of the combined triangular-quad scheme, which is depicted in figure 4.4 and for which the grid spanning matrices A and B are given in example 4.1. The system of linear equations in 4.3.1 that provides the solution x_B for the weight stencil representative

at $(0,0) \in A\mathbb{Z}^2$ of the uniform triangular scheme is

$$\left(\begin{array}{cc|ccc|cc} 1 & 1 & 1 & 1 & 1 & 1 & 1 \\ \hline \frac{1}{2} & -\frac{1}{2} & 1 & 0 & -1 & \frac{1}{2} & -\frac{1}{2} \\ -1 & -1 & 0 & 0 & 0 & 1 & 1 \\ \hline 0 & 0 & \frac{3}{4} & -\frac{1}{4} & \frac{3}{4} & 0 & 0 \\ -\frac{1}{2} & \frac{1}{2} & 0 & 0 & 0 & \frac{1}{2} & -\frac{1}{2} \\ \frac{2}{3} & \frac{2}{3} & -\frac{1}{3} & -\frac{1}{3} & -\frac{1}{3} & \frac{2}{3} & \frac{2}{3} \end{array}\right) \left(\begin{array}{c} \frac{1}{16} \\ \hline \frac{1}{16} \\ \hline \frac{1}{16} \\ \frac{5}{8} \\ \hline \frac{1}{16} \\ \hline \frac{1}{16} \\ \frac{1}{16} \end{array}\right) = \left(\begin{array}{c} 1 \\ \hline 0 \\ 0 \\ \hline -\frac{1}{16} \\ 0 \\ -\frac{1}{12} \end{array}\right)$$

already partitioned according to the degree of the monomials and the stencil support as in expression 4.3.3.

Monomials up to degree 2 are involved. The first row shows $Q_B(1) \equiv 1$ sampled over the support. The collection of $Q_B(f)$ for the two linear monomials sampled over the grid reproduces the grid itself. Hence, we may interpret rows 2 and 3 as the support Λ_B. Note, that the vector x_B is symmetric with respect to the support, as well as the entries of the three bottom rows of the matrix. The latter correspond to evaluations of $Q_B(f)$ for monomials f of degree two over the support.

According to the split carried out in 4.3.5, we remove the first two columns of the matrix, multiply the weights on the boundary and the vector on the rhs by $\frac{1}{2}$ and insert the half-sided momentum $\varpi_{|1|,(0,0)}$ computed in example 4.3 in columns 2 and 3 of the rhs. This leaves us with

$$\left(\begin{array}{ccc|cc} 1 & 1 & 1 & 1 & 1 \\ \hline 1 & 0 & -1 & \frac{1}{2} & -\frac{1}{2} \\ 0 & 0 & 0 & 1 & 1 \\ \hline \frac{3}{4} & -\frac{1}{4} & \frac{3}{4} & 0 & 0 \\ 0 & 0 & 0 & \frac{1}{2} & -\frac{1}{2} \\ -\frac{1}{3} & -\frac{1}{3} & -\frac{1}{3} & \frac{2}{3} & \frac{2}{3} \end{array}\right) \left(\begin{array}{c} \frac{1}{32} \\ \frac{5}{16} \\ \frac{1}{32} \\ \hline \frac{1}{16} \\ \frac{1}{16} \end{array}\right) = \left(\begin{array}{c} \frac{1}{2} \\ \hline 0 \\ \frac{1}{8} \\ \hline -\frac{1}{32} \\ 0 \\ -\frac{1}{24} \end{array}\right).$$

The split for the stencil around $0 \in B\mathbb{Z}^2$ on the quad side appears as

$$\left(\begin{array}{ccc|ccc} 1 & 1 & 1 & 1 & 1 & 1 \\ \hline 1 & 0 & -1 & 1 & 0 & -1 \\ -1 & -1 & -1 & 0 & 0 & 0 \\ \hline \frac{2}{3} & -\frac{1}{3} & \frac{2}{3} & \frac{2}{3} & -\frac{1}{3} & \frac{2}{3} \\ -1 & 0 & 1 & 0 & 0 & 0 \\ \frac{2}{3} & \frac{2}{3} & \frac{2}{3} & -\frac{1}{3} & -\frac{1}{3} & -\frac{1}{3} \end{array}\right) \left(\begin{array}{c} \frac{1}{64} \\ \frac{3}{32} \\ \frac{1}{64} \\ \hline \frac{3}{64} \\ \frac{9}{32} \\ \frac{3}{64} \end{array}\right) = \left(\begin{array}{c} \frac{1}{2} \\ \hline 0 \\ -\frac{1}{8} \\ \hline -\frac{1}{24} \\ 0 \\ -\frac{1}{24} \end{array}\right).$$

Since the boundary support of both stencils is $\Lambda_A^0 = \Lambda_B^0 = \{(1,0),(0,0),(-1,0)\}$, we manage to reduce the matrix $[M_{Q_A(\Lambda_A^0)} \mid M_{Q_B(\Lambda_B^0)}]$ from 6 to 3 columns. The solution for the weight stencil at $0 \in g(A,B)$ is then apparent in

$$\left(\begin{array}{ccc|ccc|cc} 1 & 1 & 1 & 1 & 1 & 1 & 1 & 1 \\ \hline 1 & 0 & -1 & 1 & 0 & -1 & \frac{1}{2} & -\frac{1}{2} \\ -1 & -1 & -1 & 0 & 0 & 0 & 1 & 1 \\ \hline \frac{2}{3} & -\frac{1}{3} & \frac{2}{3} & \frac{17}{24} & -\frac{7}{24} & \frac{17}{24} & 0 & 0 \\ -1 & 0 & 1 & 0 & 0 & 0 & \frac{1}{2} & -\frac{1}{2} \\ \frac{2}{3} & \frac{2}{3} & \frac{2}{3} & -\frac{1}{3} & -\frac{1}{3} & -\frac{1}{3} & \frac{2}{3} & \frac{2}{3} \end{array}\right) \left(\begin{array}{c} \frac{1}{64} \\ \frac{3}{32} \\ \frac{1}{64} \\ \hline \frac{5}{64} \\ \frac{19}{32} \\ \frac{5}{64} \\ \hline \frac{1}{16} \\ \frac{1}{16} \end{array}\right) = \left(\begin{array}{c} 1 \\ \hline 0 \\ 0 \\ \hline -\frac{7}{96} \\ 0 \\ -\frac{1}{12} \end{array}\right) \tag{4.3.12}$$

as the "average" of the two uniform stencils.

Remark 4.4. The reason why for two schemes that seperately reproduce cubic polynomials the combined scheme might not is that grid spanning matrices of $g(A,B)$ such that the half-sided moments of order 1 and 3 match simultaneously do not exist. The half-sided moments of even order do not harm the construction given symmetric support.

So far, we have ensured, that weights on the boundary can be averaged from the weights of the two uniform schemes along the boundary as seen in figure 4.4.

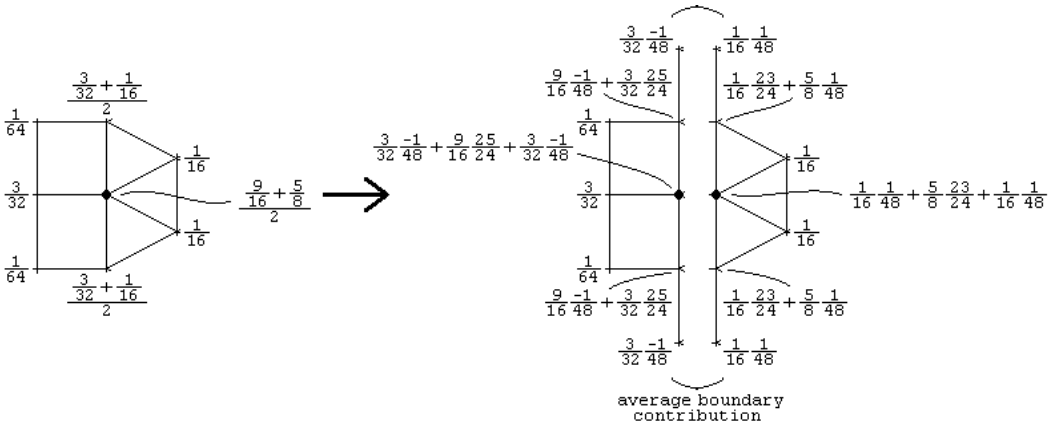

Figure 4.5 : Averaging the weights for stencils at boundary points is preceeded by the application of convolution operators for a selected stencil from the triangular-quad scheme.

Recall that to validly subdivide points close to the boundary a convolution operator is applied along the boundary. In view of a simple implementation it is desirable to first convolve the boundary points and then apply weight stencils combined by ordinary weights over the entire mesh. Figure 4.5 illustrates this principle for a stencil at a point on the boundary of the triangular-quad scheme. Hence, we establish the last small result.

Remark 4.5. Note, that lemma 4.1 applies to each of the systems of linear equations in 4.3.4 and 4.3.5 that are here restated as

$$[\ M_{Q_A(\Lambda_A^-)} \mid M_{Q_A(\Lambda_A^0)}\ ] \cdot [\ x_A^- \mid \frac{1}{2}x_A^0\ ] = \bar{b}_A$$

and

$$[\ M_{Q_B(\Lambda_B^0)} \mid M_{Q_B(\Lambda_B^+)}\ ] \cdot [\ \frac{1}{2}x_B^0 \mid x_B^+\ ] = \bar{b}_B.$$

Suppose the ordinary supports restricted to the boundary satisfy $\Lambda^0 = \Lambda_A^0 = \Lambda_B^0$. Then lemma 4.1 grants a solution of the following form

$$[\ M_{Q_A(\Lambda_A^-)} \mid M_{\frac{1}{2}(Q_A+Q_B)(\hat{\Lambda})}\ ] \left(\begin{array}{c|c} I & 0 \\ \hline 0 & U_A \end{array}\right) \cdot [\ x_A^- \mid \frac{1}{2}x_A^0\ ] = \bar{b}_A \qquad (4.3.13)$$

$$[\ M_{\frac{1}{2}(Q_A+Q_B)(\hat{\Lambda})}\ |\ M_{Q_B(\Lambda_B^+)}\ ] \left(\begin{array}{c|c} U_B & 0 \\ \hline 0 & I \end{array}\right) \cdot [\ \frac{1}{2}x_B^0\ |\ x_B^+\ ] = \bar{b}_B \tag{4.3.14}$$

for the choice $\hat{S}^\infty = \frac{1}{2}(S_A^\infty + S_B^\infty)$ and a sufficient support extention $\hat{\Lambda}$ of Λ_0. As already noted in the proof of lemma 4.2 the identity

$$\bar{b}_A + \bar{b}_B = b_{\frac{1}{2}(Q_A+Q_B)(0)}$$

holds, so that eqs. 4.3.13 and 4.3.14 are joined to

$$M_{Q_A(\Lambda_A^-),\frac{1}{2}(Q_A+Q_B)(\hat{\Lambda}),Q_B(\Lambda_B^+)} \cdot [x_A^-\ |\ \frac{1}{2}(U_A x_A^0 + U_B x_B^0)\ |\ x_B^+] = b_{\frac{1}{2}(Q_A+Q_B)(0)}.$$

For simplicity we demanded the equality of the boundary support $\Lambda_A^0 = \Lambda_B^0$ so that the solution given by 4.3.8 does not require differentiation when multiplying with U_A and U_B. A more general term can be obtained.

4.4 Volumetric examples

In this section we demonstrate how the previously developed tools aid us to combine various pairs of uniform volumetric subdivision schemes. Since the computation is similar among all pairwise combinations, we work out the details thoroughly in the first example and proceed in a somewhat faster manner thereafter. In the second example we demonstrate that, in general, weight stencils leading to polynomial reproduction are not uniquely determined.

Example 4.5. We combine triangular prisms (A) with the tetrahedra-octahedra lattice (B) in a bi-uniform grid $g(A, B)$ with

$$A = \begin{pmatrix} 1 & -\frac{1}{2} & 0 \\ 0 & \frac{\sqrt{3}}{2} & 0 \\ 0 & 0 & 1 \end{pmatrix} \quad \text{and} \quad B = \begin{pmatrix} 1 & \frac{1}{2} & \frac{1}{2} \\ 0 & \frac{\sqrt{3}}{2} & \frac{1}{2\sqrt{3}} \\ 0 & 0 & 1 \end{pmatrix}.$$

A region of the grid is visualized in figure 4.6.b. Motivated by lemma 4.2 we design the matrices A and B so that the half-sided moments of first order for the four boundary

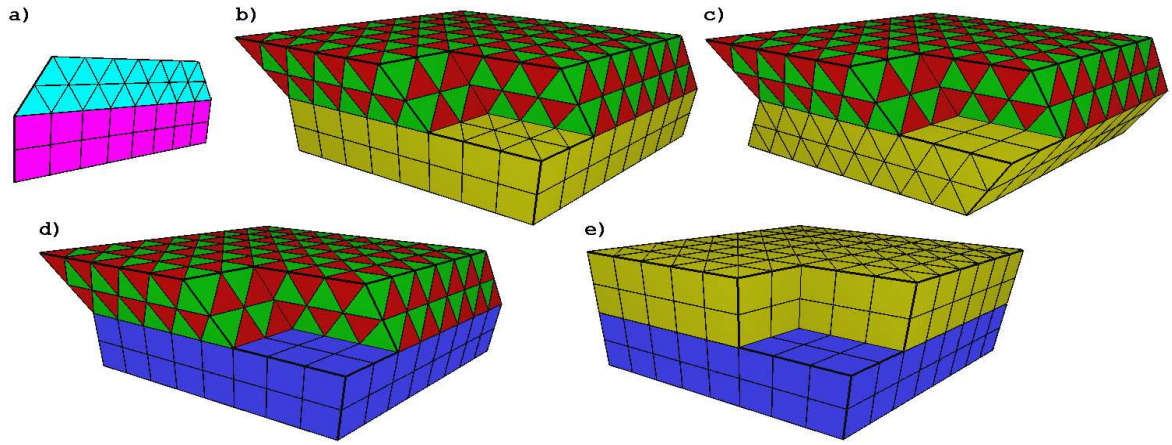

Figure 4.6 : Parts of bi-uniform grids. Subdivision rules on volumetric grids such as illustrated in b)-e) are derived in section 4.4.

weight stencil representatives match to

$$\varpi_{|1|,(0,0,0)} = \varpi_{|1|,(1,0,0)} = \varpi_{|1|,(0,1,0)} = \varpi_{|1|,(1,1,0)} = \begin{pmatrix} 0 \\ 0 \\ \frac{1}{8} \end{pmatrix}$$

for the uniform prism scheme on $A\mathbb{Z}^3$ and the uniform tetrahedral-octahedral subdivision scheme on $B\mathbb{Z}^3$. Both schemes were discussed in examples 3.1 and 3.2.

We recall that the quasi-interpolant for the uniform tetrahedral-octahedral scheme is $Q\colon \pi_3(\mathbb{R}^3) \longrightarrow \pi_3(\mathbb{Z}^3)$ with

$$Q(f) = f|_{\mathbb{Z}^3} - (\nabla \begin{pmatrix} \frac{1}{6} & -\frac{1}{18} & -\frac{1}{18} \\ -\frac{1}{18} & \frac{1}{6} & -\frac{1}{18} \\ -\frac{1}{18} & -\frac{1}{18} & \frac{1}{6} \end{pmatrix} \nabla^T f)|_{\mathbb{Z}^3}.$$

According to lemma 3.3 on the transformed uniform grid $Q_B\colon \pi_3(\mathbb{R}^3) \longrightarrow \pi_3(B\mathbb{Z}^3)$ with $Q_B(f) = f|_{B\mathbb{Z}^3} - (\nabla H_B \nabla^T f)|_{B\mathbb{Z}^3}$ in which the coefficients of the second order

derivatives are gathered in

$$H_B = \begin{pmatrix} \frac{1}{9} & 0 & 0 \\ 0 & \frac{1}{9} & 0 \\ 0 & 0 & \frac{1}{6} \end{pmatrix}.$$

Next, we consider the transformed prism grid, for which the quasi-interpolant operator is taken from expression 3.2.5, though the dimensions are permuted according to (1 2 3) $\longrightarrow$ (2 3 1) so that triangular subdivision is performed in the first two dimensions and cubic B-spline subdivision orthogonal to the boundary. Therefore the operator $Q\colon \pi_3(\mathbb{R}^3) \longrightarrow \pi_3(\mathbb{Z}^3)$ is modified to

$$Q(f) = f|_{\mathbb{Z}^3} - (\nabla \begin{pmatrix} \frac{1}{6} & \frac{1}{12} & 0 \\ \frac{1}{12} & \frac{1}{6} & 0 \\ 0 & 0 & \frac{1}{6} \end{pmatrix} \nabla^T f)|_{\mathbb{Z}^3},$$

which yields $Q_A\colon \pi_3(\mathbb{R}^3) \longrightarrow \pi_3(A\mathbb{Z}^3)$ with $Q_A(f) = f|_{A\mathbb{Z}^3} - (\nabla H_A \nabla^T f)|_{A\mathbb{Z}^3}$ where

$$H_A = \begin{pmatrix} \frac{1}{8} & 0 & 0 \\ 0 & \frac{1}{8} & 0 \\ 0 & 0 & \frac{1}{6} \end{pmatrix}.$$

In view of combining the two schemes, we define $Q\colon \pi_2(\mathbb{R}^s) \longrightarrow l(g(A,B))$ as

$$Q(f)(x) = \begin{cases} f(x) - (\nabla H_A \nabla^T f)(x) & x_s < 0 \\ \hat{Q}(f)(x) & x_s = 0 \\ f(x) - (\nabla H_B \nabla^T f)(x) & x_s > 0 \end{cases} \qquad \forall x \in g(A,B).$$

For the boundary we choose $\hat{Q}\colon \pi_2(\mathbb{R}^2) \longrightarrow \pi_2(g(A,B))$ as

$$\hat{Q}(f) = (f - \nabla \frac{1}{2}(H_A + H_B)\nabla^T f)|_{g(A,B)},$$

i.e. the average of the quasi-interpolants Q_A and Q_B. The ordinary weight stencils are known for each uniform scheme, they apply away from the boundary. As soon as a stencil support touches, but does not overlap the boundary, lemma 4.1 suggests

to precede subdivision by applying one of the two appropriate convolution operators along the boundary $A(\mathbb{Z}^2 \times \{0\})$, for which we will now derive the masks. For a stencil at a point on the boundary remark 4.5 applies. The enumeration is complete because each ordinary stencil is supported at most over the one-ring.

In the two extraordinary cases, the support Λ involves points from the boundary, denoted by $\Lambda^0 \neq \emptyset$, and we join the set $\hat{\Lambda}$ to the support so that $\hat{\Lambda}$ computes $Q_A\hat{S}^\infty$ and $Q_B\hat{S}^\infty$ at the values of Λ^0 for polynomials up to degree 2. Recall also illustrations 4.3 and 4.5 on stencil support extention for the bivariate setting. Therefore, we obtain

$$\begin{aligned} Q_A\hat{S}^\infty &= (Id - \nabla H_A \nabla^T)(Id + \frac{1}{2}\nabla(H_A + H_B)\nabla^T) \\ &= Id + \nabla(\frac{H_A + H_B}{2} - H_A)\nabla^T \\ &= Id + \nabla \begin{pmatrix} -\frac{1}{144} & 0 & 0 \\ 0 & -\frac{1}{144} & 0 \\ 0 & 0 & 0 \end{pmatrix} \nabla^T. \end{aligned}$$

The boundary region of $g(A, B)$ is extracted as $\begin{pmatrix} 1 & -\frac{1}{2} \\ 0 & \frac{\sqrt{3}}{2} \end{pmatrix} \mathbb{Z}^2$, on which according to expression and support Θ in 2.4.5 the operator $Q_A\hat{S}^\infty$ is expressed by the discrete convolution operator defined by the mask

$$\nu_A|_\Theta = \begin{pmatrix} 0 & 0 & \\ 0 & 1 & 0 \\ 0 & 0 & \end{pmatrix} + \frac{-1}{144} \begin{pmatrix} & \frac{2}{3} & \frac{2}{3} & \\ \frac{2}{3} & -4 & \frac{2}{3} \\ & \frac{2}{3} & \frac{2}{3} & \end{pmatrix} = \begin{pmatrix} & \frac{-1}{216} & \frac{-1}{216} & \\ \frac{-1}{216} & \frac{37}{36} & \frac{-1}{216} \\ & \frac{-1}{216} & \frac{-1}{216} & \end{pmatrix}.$$

Note, that $Q_A\hat{S}^\infty$ contains no partial derivatives involving the variable x_3, i.e. orthogonal to the boundary.

The operator $Q_B\hat{S}^\infty$ reduces to

$$\begin{aligned} Q_B\hat{S}^\infty &= (Id - \nabla H_B \nabla^T)(Id + \frac{1}{2}\nabla(H_A + H_B)\nabla^T) \\ &= Id + \nabla(\frac{H_A + H_B}{2} - H_B)\nabla^T \\ &= Id + \nabla \begin{pmatrix} \frac{1}{144} & 0 & 0 \\ 0 & \frac{1}{144} & 0 \\ 0 & 0 & 0 \end{pmatrix} \nabla^T, \end{aligned}$$

equivalently expressed by convolution with the mask

$$\nu_B|_\Theta = \begin{pmatrix} & 0 & 0 & \\ 0 & 1 & 0 & \\ & 0 & 0 & \end{pmatrix} + \frac{1}{144} \begin{pmatrix} & \frac{2}{3} & \frac{2}{3} & \\ \frac{2}{3} & -4 & \frac{2}{3} & \\ & \frac{2}{3} & \frac{2}{3} & \end{pmatrix} = \begin{pmatrix} & \frac{1}{216} & \frac{1}{216} & \\ \frac{1}{216} & \frac{35}{36} & \frac{1}{216} & \\ & \frac{1}{216} & \frac{1}{216} & \end{pmatrix}. \qquad (4.4.1)$$

Notice that the operators $Q_A\hat{S}^\infty$ and $Q_B\hat{S}^\infty$ differ only by an intermediate sign, which is due to the special form of $\hat{Q}$.

We conclude that due to the shape of Θ, the boundary part of the support Λ^0 of a weight stencil needs to be extended to the one-environment of Λ^0 restricted to the boundary.

In most combinations of two subdivision schemes on a bi-uniform grid $g(A, B)$ essentially different choices for the grid spanning matrices A and B are possible, as demonstrated in

Example 4.6. We consider the quads of the uniform prism grid touching the uniform tetrahedral-octahedral grid along a common uniform boundary. Each quad of a prism is then touched by a triangular face of a tetrahedron and an octahedron as illustrated in 4.6.c.

Two choices for boundary alignment enumerate as follows: In the first case, let the grid $g_1(A, B)$ be generated by

$$A = \begin{pmatrix} 1 & 0 & -\frac{1}{2} \\ 0 & 1 & 0 \\ 0 & 0 & 1 \end{pmatrix} \qquad \text{and} \qquad B = \begin{pmatrix} 1 & 0 & \frac{1}{3} \\ 0 & 1 & \frac{1}{3} \\ 0 & 0 & 1 \end{pmatrix}$$

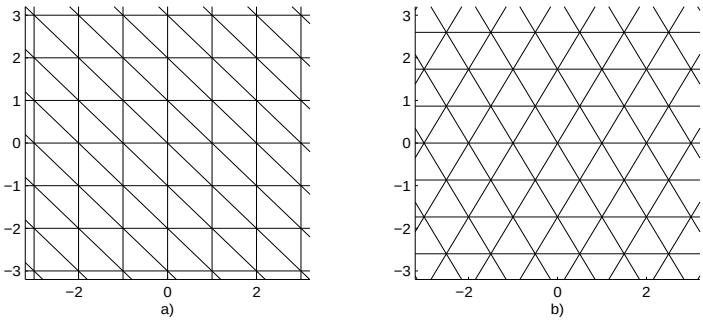

Figure 4.7 : Possible choices for boundary alignment when combining the quads of prisms with the triangles of the tetrahedral-octahedral mesh. In the left image the quads remain in their natural embedding, whereas in the right the triangles are aligned in their equilateral configuration.

in which the boundary $A(\mathbb{Z}^2 \times \{0\})$ is spanned by the first two unit vectors, as displayed in figure 4.7.a. The diagonals indicate additional edges induced by the subdivision weights between tetrahedra and octahedra. The matrices that represent the linear combination of second order derivatives in the quasi-interpolants of the uniform schemes can be computed with aid of lemma 3.3:

$$H_A = \begin{pmatrix} \frac{1}{8} & 0 & 0 \\ 0 & \frac{1}{6} & 0 \\ 0 & 0 & \frac{1}{6} \end{pmatrix} \qquad \text{and} \qquad H_B = \begin{pmatrix} \frac{4}{27} & \frac{-2}{27} & 0 \\ \frac{-2}{27} & \frac{4}{27} & 0 \\ 0 & 0 & \frac{1}{6} \end{pmatrix}.$$

Discretizing the non-vanishing partial derivatives together with the identity in the operators $Q_A\hat{S}^\infty$ and $Q_B\hat{S}^\infty$ yields the masks

$$\nu_A|_{[-1,1]^2} = \begin{pmatrix} \frac{1-\zeta}{54} & \frac{4\zeta-1}{108} & \frac{-1-\zeta}{54} \\ \frac{5+16\zeta}{432} & 1+\frac{-1-16\zeta}{216} & \frac{5+16\zeta}{432} \\ \frac{-1-\zeta}{54} & \frac{4\zeta-1}{108} & \frac{1-\zeta}{54} \end{pmatrix}, \nu_B|_{[-1,1]^2} = \begin{pmatrix} \frac{\zeta-1}{54} & \frac{1-4\zeta}{108} & \frac{1+\zeta}{54} \\ \frac{-5-16\zeta}{432} & 1+\frac{1+16\zeta}{216} & \frac{-5-16\zeta}{432} \\ \frac{1+\zeta}{54} & \frac{1-4\zeta}{108} & \frac{\zeta-1}{54} \end{pmatrix}$$

that must be applied to the boundary control points before subdividing with ordinary weight stencils. $\nu_B|_{[-1,1]^2}$ where $\zeta = 0$ is displayed in figure 4.8.c1.

As a second possibility for an embedding of the combined scheme to $g_2(A, B)$, we

define A and B as

$$A = \begin{pmatrix} 1 & \frac{1}{2} & -\frac{1}{2} \\ 0 & \frac{\sqrt{3}}{2} & 0 \\ 0 & 0 & 1 \end{pmatrix} \qquad \text{and} \qquad B = \begin{pmatrix} 1 & \frac{1}{2} & \frac{1}{2} \\ 0 & \frac{\sqrt{3}}{2} & \frac{1}{2\sqrt{3}} \\ 0 & 0 & 1 \end{pmatrix}$$

and achieve sheared quads vs. equilateral triangles on the boundary as displayed in figure 4.7.b. This choice results in the convolution masks

$$\nu_A|_\Theta = \begin{pmatrix} & \frac{1}{27} & \frac{-5}{108} & \\ \frac{-11}{432} & \frac{77}{72} & \frac{-11}{432} \\ & \frac{-5}{108} & \frac{1}{27} & \end{pmatrix} \qquad \text{and} \qquad \nu_B|_\Theta = \begin{pmatrix} & \frac{-1}{27} & \frac{5}{108} & \\ \frac{11}{432} & \frac{67}{72} & \frac{11}{432} \\ & \frac{5}{108} & \frac{-1}{27} & \end{pmatrix}$$

of which $\nu_B|_\Theta$ is depicted in figure 4.8.c2.

In the following examples, we visit additional combined schemes, where the boundary is patched by quads from one side and by triangles from the other. We have seen in the previous example that the support extention for the subdivision weights is somewhat smaller when shearing the quads to meet the triangles on the equilateral triangular grid as illustrated in the right of figure 4.7. The support for the convolution masks is then Θ from expression 2.4.5 instead of $[-1,1]^2$. This support might be considered advantageous for implementation. Hence, we restrict attention to these boundary configurations.

Example 4.7. The tetrahedral-octahedral scheme (A) is combined with the uniform scheme for cubes (B) discussed in example 3.3 on the grid $g(A,B)$. The generating matrices are

$$A = \begin{pmatrix} 1 & \frac{1}{2} & \frac{1}{2} \\ 0 & \frac{\sqrt{3}}{2} & \frac{1}{2\sqrt{3}} \\ 0 & 0 & 1 \end{pmatrix} \qquad \text{and} \qquad B = \begin{pmatrix} 1 & \frac{1}{2} & 0 \\ 0 & \frac{\sqrt{3}}{2} & 0 \\ 0 & 0 & 1 \end{pmatrix}.$$

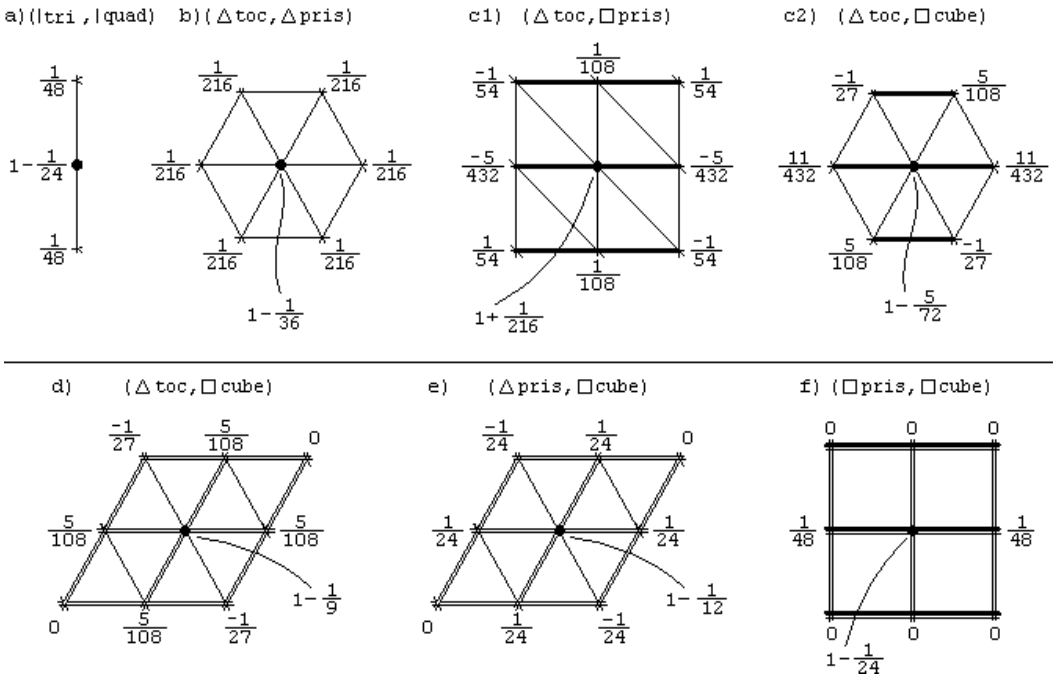

Figure 4.8 : Convolution masks for various pairwise combinations of uniform subdivision schemes to apply on the boundary of $g(A, B)$. Thick lines indicate edge-adjacent triangles of prism; double lines indicate edge-adjacent quads of cube.

Analogous to the computations in the first example of this section 4.5 we obtain

$$\nu_A|_\Theta = \begin{pmatrix} \frac{-1}{27} & \frac{5}{108} & \\ \frac{5}{108} & \frac{8}{9} & \frac{5}{108} \\ & \frac{5}{108} & \frac{-1}{27} \end{pmatrix} \qquad \text{and} \qquad \nu_B|_\Theta = \begin{pmatrix} \frac{1}{27} & \frac{-5}{108} & \\ \frac{-5}{108} & \frac{10}{9} & \frac{-5}{108} \\ & \frac{-5}{108} & \frac{1}{27} \end{pmatrix}$$

of which $\nu_A|_\Theta$ is displayed in figure 4.8.d.

Example 4.8. We align the triangular boundary of the uniform prism grid (A) with the quads of the cube scheme (B). A region of the bi-uniform grid $g(A, B)$ is displayed in figure 4.6.d where the matrices are chosen to be

$$A = \begin{pmatrix} 1 & -\frac{1}{2} & 0 \\ 0 & \frac{\sqrt{3}}{2} & 0 \\ 0 & 0 & 1 \end{pmatrix} \qquad \text{and} \qquad B = \begin{pmatrix} 1 & \frac{1}{2} & 0 \\ 0 & \frac{\sqrt{3}}{2} & 0 \\ 0 & 0 & 1 \end{pmatrix}.$$

Here, the operators $Q_A\hat{S}^\infty$ and $Q_B\hat{S}^\infty$ are equivalent to the discrete convolution operators defined by the masks

$$\nu_A|_\Theta = \begin{pmatrix} \frac{-1}{24} & \frac{1}{24} & \\ \frac{1}{24} & \frac{11}{12} & \frac{1}{24} \\ & \frac{1}{24} & \frac{-1}{24} \end{pmatrix} \qquad \text{and} \qquad \nu_B|_\Theta = \begin{pmatrix} \frac{1}{24} & \frac{-1}{24} & \\ \frac{-1}{24} & \frac{13}{12} & \frac{-1}{24} \\ & \frac{-1}{24} & \frac{1}{24} \end{pmatrix}.$$

Remark 4.6. The subdivision scheme on the common boundary of a uniform prism grid connected to the uniform cube grid so that the quads of the cubes meet the quads of the prisms, follows from tensoring the triangular-quad scheme reviewed in example 4.1 with the univariate B-spline scheme. The resulting convolution mask displayed in figure 4.8.f resembles therefore the mask of the triangular-quad scheme.

That the combined scheme produces globally C^2 limit functions follows from the fact that both the triangular-quad scheme and the univariate cubic B-spline scheme are of class C^2.

The support of the weight stencils of the three uniform schemes, tetrahedral-octahedral, prism and cube, are symmetric when aligned around zero. Each support

does not exceed the one-ring. The half sided moments of order 1 of all transformed uniform schemes in examples 4.6–8 for the four boundary weight stencil representatives are

$$\varpi_{|1|,(0,0,0)} = \varpi_{|1|,(1,0,0)} = \varpi_{|1|,(0,1,0)} = \varpi_{|1|,(1,1,0)} = \begin{pmatrix} 0 \\ 0 \\ \frac{1}{8} \end{pmatrix}.$$

Hence, either lemma 4.1 or remark 4.5 applies, when ordinary stencil support involves the boundary. We can assure that after applying the two convolution masks on the common boundary and creating duplicates of the boundary control points, to which we refer from now on as *unzipping*, one round of subdivision is completed by applying ordinary weight stencils or an averaged combination of these stencils.

4.5 Smoothness analysis

[$L^2$03] developed an analysis procedure to prove smoothness properties of a subdivision scheme. The technique is referred to as the *joint spectral radius test* and applies to uniform schemes as well as combined subdivision schemes. The test can assert that for a particular scheme the m-th degree Taylor expansion coefficients of any limit function on an appropriate dense diadic point set are uniformly bounded, which guarantees that the scheme is of class C^m.

In the following, we revisit the four combined volumentric schemes derived in the previous section and check whether they produce globally $S^\infty P_0 \in C^2$ limit functions, i.e. including the crucial region of the boundary and environment, for all possible initial control point assignments $P_0 \in l(g(A, B))$. Therefore, it is necessary that each of the uniform volumetric subdivision schemes is of class C^2.

We set up the joint spectral radius test for each combined volumetric scheme over the grid $g(A, B)$ to prove that the 2-nd degree Taylor expansion coefficients at the diadic points of the boundary interval

$$\Upsilon = A([0, 1]^2 \times \{0\})$$

are uniformly bounded. The set Υ is also described by the convex hull of the four vectors $\tau_1 = 0$, $\tau_2 = A_{:,1}$, $\tau_3 = A_{:,2}$ and $\tau_4 = \tau_2 + \tau_3$.

In order to perform the test, we fix the support $\Lambda = \left\{\lambda_1, ..., \lambda_{|\Lambda|}\right\} \subset g(A, B)$ so that the limit function $S^\infty P_0$ restricted over the subset $A([0,1]^2 \times [-1,1]) \subset \mathbb{R}^3$ depends only on values $P_0|_\Lambda$ and so that $(SP_0)|_{\Lambda+\tau_i}$ for $i = 1...4$, i.e. the values of the control points after one round of subdivision at $\Lambda + \tau_i$, depend only on the control points $P_0|_\Lambda$. Figure 4.6.b–e displays the extent of a feasible choice for Λ for each of the four combined schemes, when reattaching the removed rectangular solid and centering the lattice around the origin.

Let $\delta_\lambda \in l(g(A, B))$ be the set of control points with $\delta(\lambda) = 1$ and zero everywhere else. With the finite set Λ we are able to capture the behaviour of each scheme over Υ in matrix form in the sense that for an initial set of control points P_0 the value of the limit function at a diadic point d in Υ is obtained as the matrix product

$$(S^\infty P_0)(d) = ...M_{\varepsilon_3} M_{\varepsilon_2} M_{\varepsilon_1} P_0|_L \tag{4.5.1}$$

where $M_i \in \mathbb{R}^{|\Lambda| \times |\Lambda|}$ with

$$(M_i)_{(j,k)} = (S\delta_{\lambda_k})(\lambda_j + \tau_i) \qquad j, k \in \{1, ..., |\Lambda|\}, \quad i \in \{1, ..., 4\}$$

and $\varepsilon \in \{1, 2, 3, 4\}^{\mathbb{N}}$ depending on the bivariate diadic expansion of d.

In order to yield an iteration that converges to the Taylor expansion coefficients of the limit function $S^\infty P_0$ of up to order 2, we perform a change of basis. Due to the relation

$$SQx^j = Q\sigma x^j = 2^{|j|} Qx^j \qquad \forall j \text{ with } 0 \leq |j| \leq 2$$

obtained by corollary 2.3.3 where $X = g(A, B)$ the element $Qx^j \in l(g(A, B))$ is an eigenfunction corresponding to the eigenvalue $2^{|j|}$ of the operator S. Now we restrict S and the known eigenfunctions to the support Λ and define

$$E_k = [\ (Qx^j)|_\Lambda \ \mid \ 0 \leq j \text{ and } |j| = k\ ]$$

as the concatenation of $Qf|_\Lambda$ for all monomials f of degree k. Performing a change of basis of the subdivision matrices to

$$\tilde{M}_i = V^{-1} M_i V \qquad i \in \{1, ..., 4\},$$

where $V \in \mathbb{R}^{|\Lambda|\times|\Lambda|}$ is a concatenation of the rectangular matrices E_0, E_1 and E_2 with the nullspace of $[E_0 \mid E_1 \mid E_2]^T$ leaves each $\tilde{M}_i$ in the form

$$\tilde{M}_i = \left(\begin{array}{c|c} \Theta_i & C_i \\ \hline 0 & Y_i \end{array}\right).$$

In this expression the submatrix $\Theta_i \in \mathbb{R}^{10\times 10}$ for $i \in \{1, ..., 4\}$ has the structure

$$\Theta_i = \left(\begin{array}{c|ccc|cccccc} 1 & * & * & * & * & * & * & * & * & * \\ \hline 0 & \frac{1}{2} & 0 & 0 & * & * & * & * & * & * \\ 0 & 0 & \frac{1}{2} & 0 & * & * & * & * & * & * \\ 0 & 0 & 0 & \frac{1}{2} & * & * & * & * & * & * \\ \hline 0 & 0 & 0 & 0 & \frac{1}{4} & 0 & 0 & 0 & 0 & 0 \\ 0 & 0 & 0 & 0 & 0 & \frac{1}{4} & 0 & 0 & 0 & 0 \\ 0 & 0 & 0 & 0 & 0 & 0 & \frac{1}{4} & 0 & 0 & 0 \\ 0 & 0 & 0 & 0 & 0 & 0 & 0 & \frac{1}{4} & 0 & 0 \\ 0 & 0 & 0 & 0 & 0 & 0 & 0 & 0 & \frac{1}{4} & 0 \\ 0 & 0 & 0 & 0 & 0 & 0 & 0 & 0 & 0 & \frac{1}{4} \end{array}\right),$$

where the $*$ indicates a possibly non-zero entry. The nullspace computation of $[E_0 \mid E_1 \mid E_2]^T$ is numerically stable, when orthonormalizing the vectors in E_k for $k = 1$ and $k = 2$.

The joint spectral radius of the set of matrices $\Sigma = \{Y_1, ..., Y_4\}$ is defined as

$$\rho_\infty(\Sigma) = \lim_{n\longrightarrow\infty} \rho_n(\Sigma),$$

i.e. the limit of the monotonically decreasing sequence

$$\rho_n(\Sigma) = \max\{\left\|Y_{\varepsilon_n} Y_{\varepsilon_{n-1}} ... Y_{\varepsilon_1}\right\| : \varepsilon \in \{1, ..., 4\}^n\}^{\frac{1}{n}}. \tag{4.5.2}$$

[$L^2$03] shows that if $\rho_n(\{Y_1, ..., Y_4\}) < \frac{1}{4}$ for some $k \in \mathbb{N}$, the combined subdivision scheme is of class C^2. We obtained

Example	$\rho_{10}(\{Y_1, ..., Y_4\})$	$\max[eig(Y_i) < \frac{1}{4}]$
4.5	0.22459...	0.1359...
4.6.b	0.21825...	0.1351...
4.7	0.21493...	0.1359...
4.8	0.20778...	$\frac{1}{8}$

Hence, each of the bi-uniform volumetric schemes derived in section 4.4 yields limit functions over $\mathbb{R}^3$ that are two times differentiable. The interested reader may obtain the matrices M_i as well as Y_i for the four schemes in the `mat`–format from

`www.subdivision.org/jsr_vol.zip`

Remark 4.7. The choice of the matrix V has great influence on the rate of convergence of the sequence $\rho_n(\{Y_1, ..., Y_4\})$. The number of multiplications can be lowered from $4^n(n-1)$ using intermediate results at the expense of storage. [ZL04] suggests also to diagonalize the matrices $\tilde{M}_i$ using further common eigenspaces to eigenvalues $< \frac{1}{4}$. Under the objective of minimizing ρ_n we found the choice of the 2-norm in equation 4.5.2 superior to the 1-norm or the ∞-norm, although computationally less efficient.

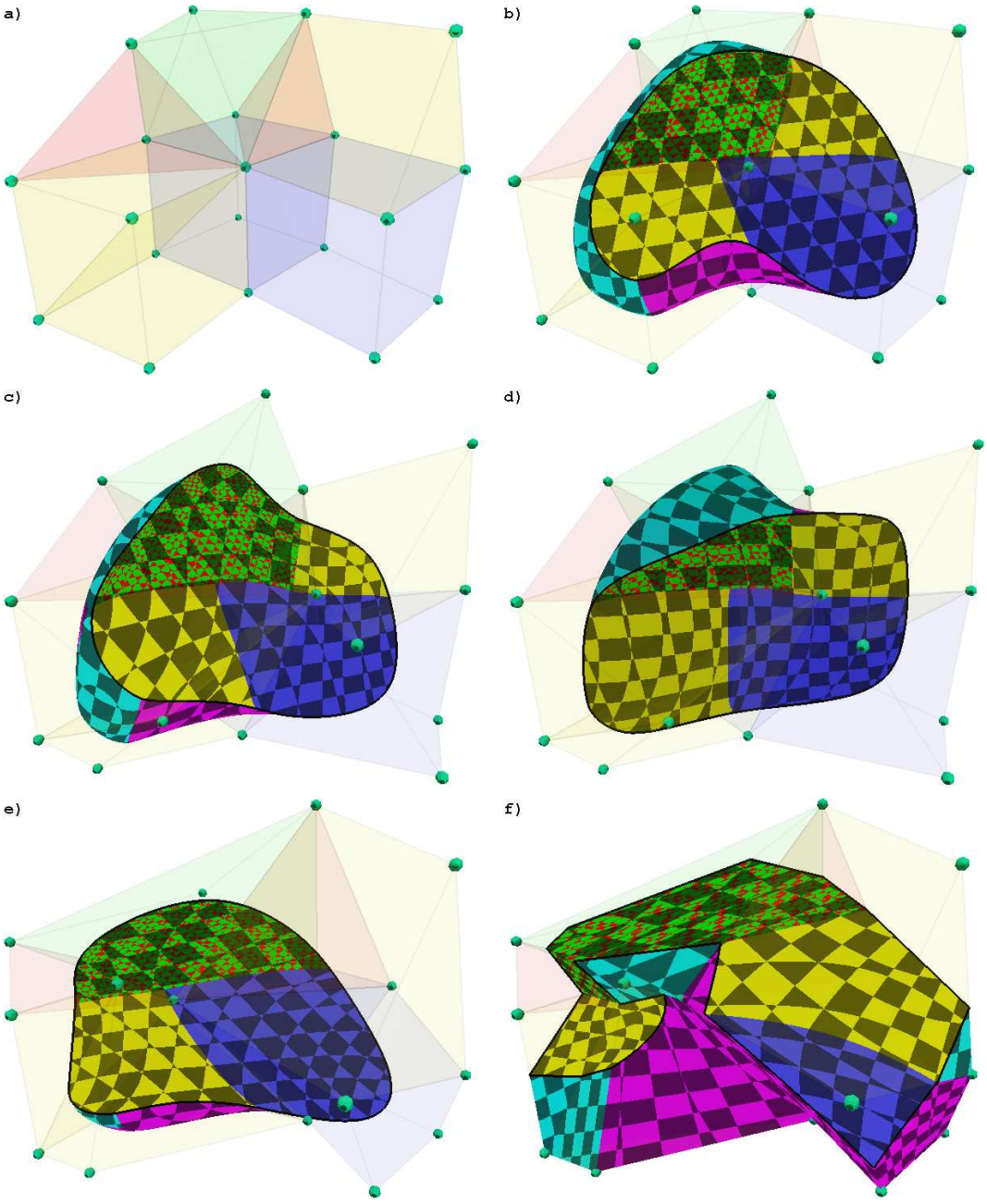

Figure 4.9 : Visualisation of smoothness using a 3d checker board texture on cross-sections of the deformed and subdivided mesh. a) shows test mesh. Texture coordinates are assigned to each vertex of subdivided mesh in b). The texture coordinate is identical to the position of the respective vertex. Various deformations in c–e). Subdivision with an algorithm of class C^0 and deformation in f).

Chapter 5

Volumetric subdivision

In this chapter we achieve the main goal of the thesis, namely to define a new volumetric subdivision scheme that operates on tetrahedra, octahedra, triangular prisms and cubes of arbitrary topology. Our subdivision scheme yields C^2 limit functions everywhere except at extraordinary edges and vertices and except where triangles of prisms touch quads of prisms.

When combining two volumetric schemes on a bi-uniform grid, examples of which are displayed in figure 4.6, we are able to choose a particular set of rules that can be interpreted as the application of two passes over the mesh: unzipping followed by ordinary subdivision rules. For control points on the boundary, the respective ordinary stencils were averaged together.

Because the ordinary subdivision rules might not be applicable at all locations of a volumetric meshes of arbitrary topology, we design one round of subdivision as three – fairly easy to implement – steps that apply globally: unzipping, linear subdivision and averaging.

On the boundary of the mesh, we apply a surface subdivision scheme. Since the boundary of our general volume mesh consists of triangles and quads, we recommend the triagular-quad scheme of [SW03] on the exterior of the mesh. We review the scheme briefly in example 5.2. The following description accounts for the remaining interior vertices, those that are entirely surrounded by volume shapes, and vertices inserted inside volume shapes.

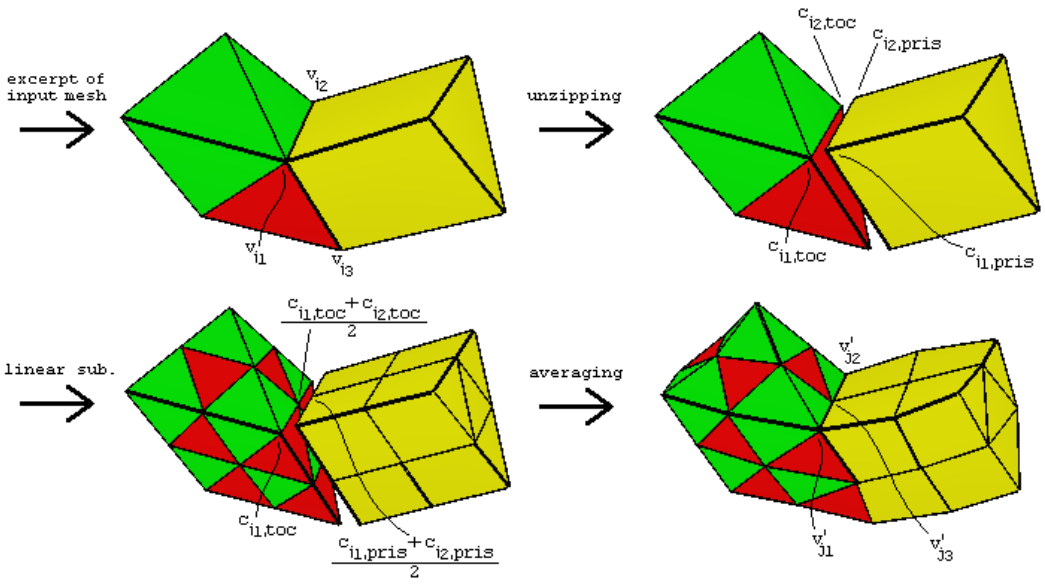

Figure 5.1 : One round of subdivision displayed at a part of an initial mesh. The vertices v_{i_1}, v_{i_2} and v_{i_3} are assumed to be entirely surrounded by volumetric shapes. The extension *toc* abbreviates "tetrahedral-octahedral". Selected vertices and clones are labeled.

5.1 Algorithm overview

One round of subdivision on a volumetric mesh of arbitrary topology is divided into three consecutive steps called (1) *unzipping*, (2) *linear subdivision* and (3) *averaging*. Thereby, the algorithm follows the principle layout already proposed in the triangular-quad paper [SW03].

In the unzipping procedure (1), we compute for each vertex v_i of the input mesh three temporary vertices

$$v_i \longrightarrow \{c_{i,toc}, c_{i,pris}, c_{i,cube}\}$$

to which we refer as clones of v_i. Their position is usually very close to the original vertex position. How precisely to generate the position of each clone is explained in detail in the next section.

Step number (2), *linear subdivision*, is a loop over all shapes, in which each tetrahe-

dron is split into 4 smaller tetrahedra and 1 octahedron. An octahedron decomposes into 8 tetrahedra and 6 tetrahedra. A triangular prism makes 8 new triangular prisms and finally a cube, splits into 8 cubes.

As suggested by figure 5.1, the vertices of the resulting shapes are computed with the corresponding clones. Inserted vertices are simply edge-midpoints, face-midpoints and inside an octahedron and a cube, a vertex as the mean of all clones of the respective shape.

For each of the four shape types, there is a characteristic matrix defined, which comes into play in procedure (3), denoted the averaging pass. In a loop over all the newly created shapes from step (2), the vertices of each shape are concatenated in a matrix, which is then multiplied by the characteristic matrix (not to be confused by the term characteristic map). From the result, we extract new vertex positions that together replace the previous vertices of the shape. Finally, vertices that might differ in position but are topologically identical, are averaged together in a simple affine combination.

As mentioned before, on the boundary of the mesh, surface subdivision is applied, not volume subdivision. Otherwise, the mesh would contract in an undesirable manner and is in the limit not C^2 almost everywhere on the exterior.

Then, one round of subdivision is complete and the output is again a volumetric mesh.

5.2 Unzipping

The convolution operators from the volumetric examples in section 4.4 are of the symbolical form

$$Id + \alpha\partial_{x_1,x_1} + \beta\partial_{x_1,x_2} + \gamma\partial_{x_2,x_2} \tag{5.2.1}$$

with small coefficients $\alpha, \beta, \gamma \in \mathbb{R}$ and where the first two dimensions, x_1 and x_2, parametrize the boundary. Expression 5.2.1 inspires our principle layout.

Unzipping a volumetric mesh means that the original position of each vertex is

distorted by affine combinations of vertices in the one-ring. In expression 5.2.1 the *Id* operator corresponds to the original vertex position. The linear combinations, in which the weights sum to zero, is due to the discretization of the partial derivatives and the factors α, β and γ.

As mentioned in the overview, for each vertex v_i unzipping outputs three clones which we denote by $c_{i,toc}$, $c_{i,pris}$, and $c_{i,cube}$. The formulas for the position of the clones are

$$\begin{aligned} c_{i,toc} &= v_i + \delta(\triangle_{toc}, \triangle_{pris})_i + \delta(\triangle_{toc}, \square_{pris})_i + \delta(\triangle_{toc}, \square_{cube})_i \\ c_{i,pris} &= v_i - \delta(\triangle_{toc}, \triangle_{pris})_i + \delta(\triangle_{pris}, \square_{cube})_i + \delta(\square_{pris}, \square_{cube})_i \\ c_{i,cube} &= v_i - \delta(\triangle_{toc}, \square_{cube})_i - \delta(\triangle_{pris}, \square_{cube})_i - \delta(\square_{pris}, \square_{cube})_i. \end{aligned} \tag{5.2.2}$$

The notation ought to suggest that only heterogeneous pairs of boundary elements of volumetric shapes adjacent to the i-th vertex contribute to the distortions δ. If a vertex is completely surrounded by shapes of one type, the three clones coincide with the vertex position v_i.

With boundary elements we refer to the 4 triangles of the surface of a tetrahedra, while each octahedron has 8 triangles as boundary elements. We consider these boundary elements to be of class *toc*. Each prism contains 2 triangles and 3 quads as boundary elements, each of which are of class *pris*. And last, the 6 quads for each cube in the mesh are of class *cube*.

A pair of boundary elements (b_1, b_2) is considered *heterogenous* whenever b_1 belongs to a different class than b_2. Quite intuitively, a pair (b_1, b_2) is called *touching*, whenever b_1 shares at least 3 vertices with b_2.

Since a boundary element of triangular prisms is either a triangle or a quad, we distinguish between the four boundary types

$$\triangle_{toc},\ \triangle_{pris},\ \square_{pris},\ \square_{cube}.$$

In eqs. 5.2.2 the vector $\delta(\triangle_{toc}, \triangle_{pris})_i$ represents the distortion at the i-th vertex caused by a tetrahedral–octahedral boundary touching triangles of a prism. We

compute $\delta(\triangle_{toc}, \triangle_{pris})_i$ in the following way. Let there be n distinct boundary pairs $(b_1, b_2)_k$ with $k = 1...n$ that satisfy b_1 is a triangle of type $\triangle_{toc}$ adjacent to vertex v_i and touching b_2, which is of type $\triangle_{pris}$, i.e. triangular boundary of a prism. We arrange the three vertices of triangle b_1 of the k-th pair in a 3×3 matrix $M_k = [v_i|v_{p_k}|v_{q_k}]$ for appropriate but interchangeable vertex indices p_k and q_k. Then

$$\delta(\triangle_{toc}, \triangle_{pris})_i = \begin{cases} 0 & n = 0 \\ \frac{1}{n}\sum_{k=1}^{n} M_k \begin{pmatrix} -\frac{1}{36} \\ \frac{1}{72} \\ \frac{1}{72} \end{pmatrix} & n > 0. \end{cases}$$

For instance in figure 5.1 the triangle $(v_{i_1}, v_{i_2}, v_{i_3})$ is a boundary of class *toc* and as a boundary of class *pris* and thus contributes to $\delta(\triangle_{toc}, \triangle_{pris})_{i_l}$ for $l = 1...3$ at the three vertices.

The other distortions are a little more complicated to obtain, but follow the same idea of contributing boundary pairs.

The vector $\delta(\triangle_{toc}, \square_{pris})_i$ is the distortion caused by tetrahedral-octahedral boundary touching quads of triangular prisms at vertex v_i. Let there be n distinct boundary pairs $(b_1, b_2)_k$ with $k = 1...n$ that satisfy b_1 is a triangle of type $\triangle_{toc}$ adjacent to the i-th vertex and touching b_2, which is of type $\square_{pris}$. For each pair $(b_1, b_2)_k$ we distinguish between three topologically distinct configurations which are depicted on the rhs of figure 5.2.c. Of relevance is, whether vertex v_i lies opposite to the quad vertex of b_2, that is not shared with the triangle b_1. Furthermore, we detect whether v_i together with another vertex of b_1 forms an edge that is part of triangular boundary of the prism. Those edges are indicated by thickened lines in figure 5.2.c.

After we have looped over all such pairs $(b_1, b_2)_k$, we have accumulated

$$\delta(\triangle_{toc}, \square_{pris})_i = \frac{1}{n}[\sum_{k_1=1}^{\mu_1}[v_i|v_{p_{k_1}}|v_{q_{k_1}}] \begin{pmatrix} \frac{5}{144} \\ -\frac{1}{9} \\ \frac{11}{144} \end{pmatrix} + \sum_{k_2=1}^{\mu_2}[v_i|v_{p_{k_2}}|v_{q_{k_2}}] \begin{pmatrix} -\frac{31}{144} \\ \frac{11}{144} \\ \frac{5}{36} \end{pmatrix} + \sum_{k_3=1}^{\mu_3}[v_i|v_{p_{k_3}}|v_{q_{k_3}}] \begin{pmatrix} -\frac{1}{36} \\ \frac{5}{36} \\ -\frac{1}{9} \end{pmatrix}] \quad (5.2.3)$$

as the distortion term for appropriate vertex indices p_{k_l} and q_{k_l} for $l = 1...3$ in each of the three sums. The value μ_1 encodes how often the first topological case occurs at the i-th vertex and analogous for μ_2 and μ_3; we set $n = \mu_1 + \mu_2 + \mu_3$.

For the distortions $\delta(\triangle_{toc}, \square_{cube})_i$ and $\delta(\triangle_{pris}, \square_{cube})_i$ caused by boundary pairs $(b_1, b_2)_k$, we distinguish two topological distinct configurations as displayed in rhs of figure 5.2.d and 5.2.e. The criterion is simply whether vertex v_i lies opposed to the quad vertex of b_2 that is not shared by the triangle b_1. In the same notation and procedure of the previous examples we define with $n = \mu_1 + \mu_2$

$$\delta(\triangle_{toc}, \square_{cube})_i = \frac{1}{n}[\sum_{k_1=1}^{\mu_1}[v_i|v_{p_{k_1}}|v_{q_{k_1}}] \begin{pmatrix} -\frac{1}{36} \\ -\frac{1}{9} \\ \frac{5}{36} \end{pmatrix} + \sum_{k_2=1}^{\mu_2}[v_i|v_{p_{k_2}}|v_{q_{k_2}}] \begin{pmatrix} -\frac{5}{18} \\ \frac{5}{36} \\ \frac{5}{36} \end{pmatrix}] \quad (5.2.4)$$

for appropriate vertex indices p_{k_l} and q_{k_l} for $l \in \{1, 2\}$, closely resembled by the definition of

$$\delta(\triangle_{pris}, \square_{cube})_i = \frac{1}{n}[\sum_{k_1=1}^{\mu_1}[v_i|v_{p_{k_1}}|v_{q_{k_1}}] \begin{pmatrix} 0 \\ -\frac{1}{8} \\ \frac{1}{8} \end{pmatrix} + \sum_{k_2=1}^{\mu_2}[v_i|v_{p_{k_2}}|v_{q_{k_2}}] \begin{pmatrix} -\frac{1}{4} \\ \frac{1}{8} \\ \frac{1}{8} \end{pmatrix}]. \quad (5.2.5)$$

Finally, we loop over each quad at a vertex v_i that is shared by a prism and a cube. Let there be n of those quads. Exactly one edge (v_i, v_{p_k}) of the quad is part of the triangular boundary of the prism for an appropriate vertex index p_k with $k = 1...n$.

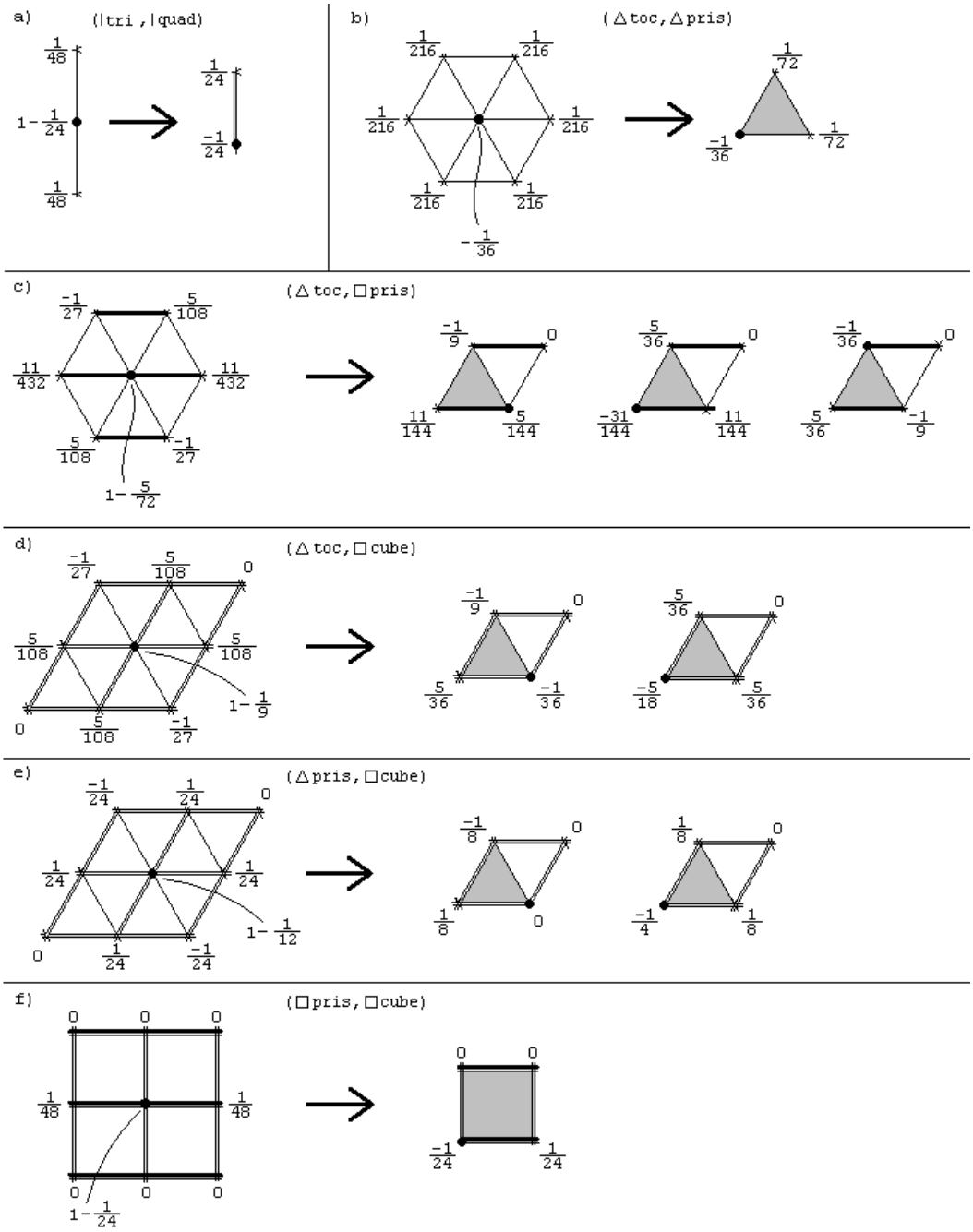

Figure 5.2 : The masks of the convolution operators are split to encode topological distinct positions of a vertex in a heterogeneous boundary pair. The masks to the right of the arrows are used in the unzipping procedure of our algorithm. Shaded regions symbolize boundary pair overlap. Thick lines indicate edge-adjacent triangles of a prism; double lines indicate edge-adjacent quads of a cube.

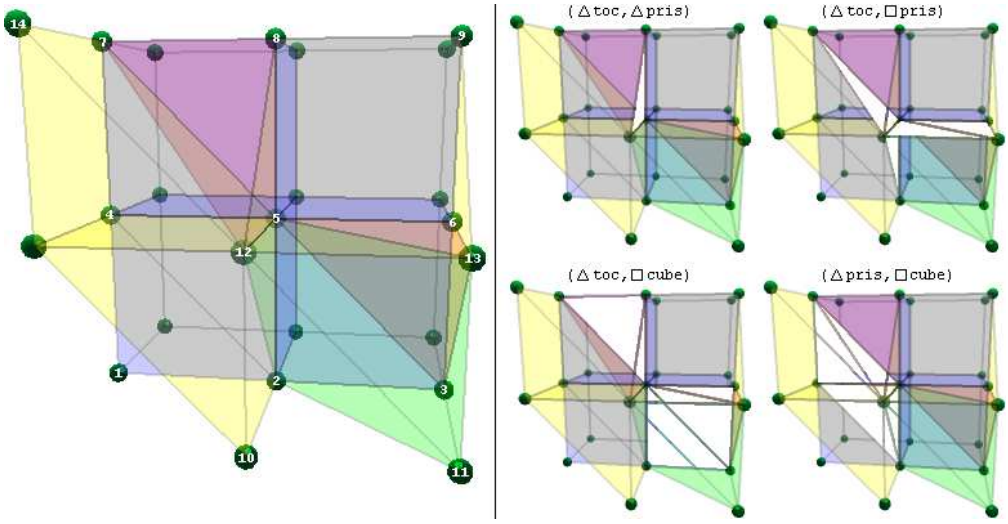

Figure 5.3 : Example mesh consists of 2 tetrahedra, 1 octahedron, 3 triangular prism, and 4 cubes. Vertices are enumerated as needed. On the right, the white faces indicate heterogeneous touching boundary pairs of the various type combinations.

Those edges around the i-th vertex contribute to

$$\delta(\square_{pris}, \square_{cube})_i = \frac{1}{n}\sum_{k=1}^{n}[v_i|v_{p_k}]\begin{pmatrix} -\frac{1}{24} \\ \frac{1}{24} \end{pmatrix} = -\frac{1}{24}v_i + \frac{1}{24n}\sum_{k=1}^{n} v_{p_k}. \tag{5.2.6}$$

For the sake of visual appearance we ommited to state until now, that each distortion is the zero vector whenever $n = 0$.

Example 5.1. Let us consider the mesh depicted in figure 5.3. We aim to compute the three clones produced by the interior vertex $v_5 \longrightarrow \{c_{5,toc}, c_{5,pris}, c_{5,cube}\}$.

Only one boundary triangle adjacent to v_5 is shared by a tetrahedra (or octahedra) and a prism. The triangle consists of the vertices (v_5, v_8, v_{12}) and contributes in $\delta(\triangle_{toc}, \triangle_{pris})_5$ as

$$\delta(\triangle_{toc}, \triangle_{pris})_5 = [v_5 \mid v_8 \mid v_{12}\,]\begin{pmatrix} -\frac{1}{36} \\ \frac{1}{72} \\ \frac{1}{72} \end{pmatrix} = -\frac{1}{36}v_5 + \frac{1}{72}(v_8 + v_{12}).$$

To obtain the distortion $\delta(\triangle_{toc}, \square_{pris})_5$ we detect that four boundary triangles of the tetrahedra and octahedra adjacent to v_5 are also part of quad boundaries of triangular prisms. Therefore

$$\begin{aligned}\delta(\triangle_{toc}, \square_{pris})_5 =& \frac{1}{4}([v_5 \mid v_{13} \mid v_{12}] \begin{pmatrix} \frac{5}{144} \\ -\frac{1}{9} \\ \frac{11}{144} \end{pmatrix} + [v_5 \mid v_7 \mid v_{12}] \begin{pmatrix} -\frac{31}{144} \\ \frac{11}{144} \\ \frac{5}{36} \end{pmatrix} \\ &+ [v_5 \mid v_2 \mid v_{12}] \begin{pmatrix} -\frac{31}{144} \\ \frac{11}{144} \\ \frac{5}{36} \end{pmatrix} + [v_5 \mid v_6 \mid v_{13}] \begin{pmatrix} -\frac{1}{36} \\ \frac{5}{36} \\ -\frac{1}{9} \end{pmatrix}),\end{aligned} \tag{5.2.7}$$

wherein the vertex ordering follows from the succeeding considerations, comparable to figure 5.3.c. The triangle (v_5, v_{13}, v_{12}) is of type $\triangle_{toc}$, whereas $(v_5, v_6, v_{13}, v_{12})$ is of type $\square_{pris}$; the two boundary elements touch because three vertices are shared. The boundary pair corresponds to the first of the three topological configurations that need to be distinguished in $\delta(\triangle_{toc}, \square_{pris})_5$, because v_5 and v_{12} form an edge of a triangular boundary of the same prism and v_5 does not lie opposite to v_6, the unoccupied vertex of the quad.

The triangle (v_5, v_7, v_{12}) is of type $\triangle_{toc}$ and $(v_5, v_7, v_{14}, v_{12})$ is of type $\square_{pris}$. The vertex v_5 lies opposite to the unoccupied vertex v_{14} of the quad. The same holds for the heterogeneous touching boundary pair consisting of (v_5, v_2, v_{12}) and $(v_5, v_2, v_{10}, v_{12})$. Both pairs are of the second topological configuration of $(\triangle_{toc}, \square_{pris})$; therefore their respective weights appear twice in expression 5.2.7.

Finally, we regard the boundary pair consisting of the triangle (v_5, v_6, v_{13}) of type $\triangle_{toc}$ and the quad $(v_5, v_6, v_{13}, v_{12})$ of type $\square_{pris}$. Neither the edge (v_5, v_6) nor the edge (v_5, v_{13}) is part of a triangular boundary of the prism; thus the weights in the rightmost picture of figure 5.2.c apply.

Next, we derive the distortion caused by a tetrahedral-octahedral boundary that touches boundaries of cubes. In each or the three distinct pairs at the 5-th vertex, v_5 does not lie opposite to the unoccupied vertex of the quad. Hence, we gather

$\delta(\triangle_{toc}, \square_{cube})_5$ as in

$$\delta(\triangle_{toc}, \square_{cube})_5 = \frac{1}{3}([v_5 \mid v_7 \mid v_8] + [v_5 \mid v_3 \mid v_6] + [v_5 \mid v_3 \mid v_2]) \begin{pmatrix} -\frac{1}{36} \\ -\frac{1}{9} \\ \frac{5}{36} \end{pmatrix}.$$

The same strategy applies to $\delta(\triangle_{pris}, \square_{cube})_5$. In our example mesh, the triangle (v_5, v_7, v_4) of type $\triangle_{pris}$ touches the quad (v_5, v_8, v_7, v_4) of type $\square_{cube}$, but v_5 does not lie opposite to v_8. The contrary is true for the pair consisting of the triangle (v_5, v_2, v_4) and the quad (v_5, v_2, v_1, v_4), in which v_5 lies opposite to v_1. Thus, we join the vertices of the two triangles to

$$\delta(\triangle_{pris}, \square_{cube})_5 = \frac{1}{2}([v_5 \mid v_7 \mid v_4] \begin{pmatrix} 0 \\ -\frac{1}{8} \\ \frac{1}{8} \end{pmatrix} + [v_5 \mid v_2 \mid v_4] \begin{pmatrix} -\frac{1}{4} \\ \frac{1}{8} \\ \frac{1}{8} \end{pmatrix}).$$

The quad (v_5, v_8, v_9, v_6) is simultaneously a boundary of a prism and a cube. Vertex v_8 is distinguished because the edge (v_5, v_8) belongs to triangular boundary of the prism. Because there is only one such quad in the mesh at v_5,

$$\delta(\square_{pris}, \square_{cube})_5 = [v_5 \mid v_8] \begin{pmatrix} -\frac{1}{24} \\ \frac{1}{24} \end{pmatrix} = -\frac{1}{24}v_5 + \frac{1}{24}v_8.$$

These distortions are substituted into equations 5.2.2 to obtain the positions of the three clones of the 5-th vertex.

In the bi-uniform mesh configuration the respective distortions reduce to the convolution operators derived in the previous chapter. Figure 5.2 illustrates how each split into the various topological configurations is motivated by the ordinary mask. The idea to distribute the weights at the center vertex so that each resulting stencil sums to zero (concerning the boundary pairs displayed in 5.2.c-e) is due to S. Schaefer. That choice greatly simplifies joining the contributions of the various topological configurations.

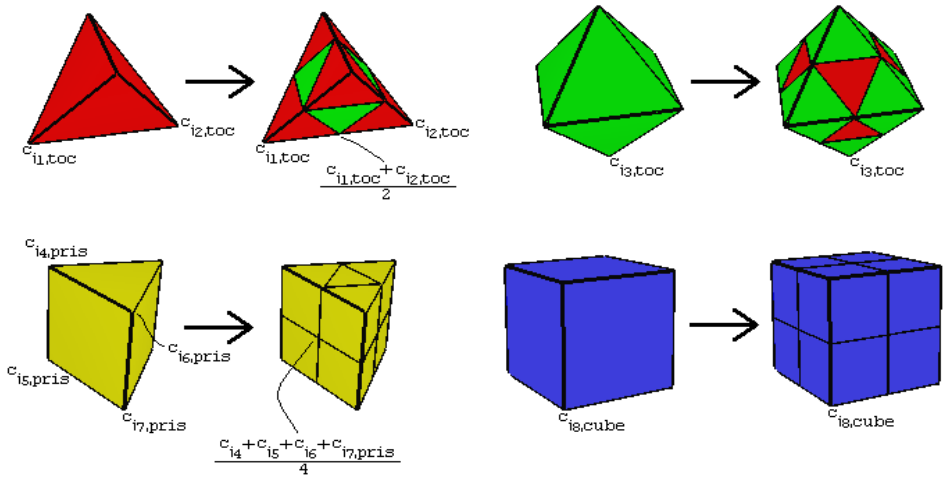

Figure 5.4 : Linear subdivision for each of the four shapes. Selected vertices are labeled and computed. Indices increase as needed. The extension *pris* is ommited for the clones c_{i_4}, c_{i_5} and c_{i_6}.

Future work will address smoothness properties of the scheme at extraordinary edges and vertices. Results on that matter might suggest modifications on how to generalize the unzipping masks from the bi-uniform schemes.

5.3 Linear subdivision and averaging

Linear subdivision and averaging is the factorization of one round of ordinary subdivision into two consecutive steps. Such factorizations were developed simultaneously in [MW01], [St01] and [ZS01].

In the volumetric scenario, linear subdivision accesses the clones and topology information of the unzipped volumetric mesh to build a new mesh. Each shape of the unzipped mesh results in multiple "smaller" shapes as displayed in figure 5.4. Vertices that appear as edge-, face- and shape-midpoints are simple affine combinations of the respective clones. Inserted vertices such as the edge-midpoints

$$w_j = \frac{c_{i_1,toc} + c_{i_2,toc}}{2} \qquad \text{and} \qquad w_k = \frac{c_{i_1,pris} + c_{i_2,pris}}{2}$$

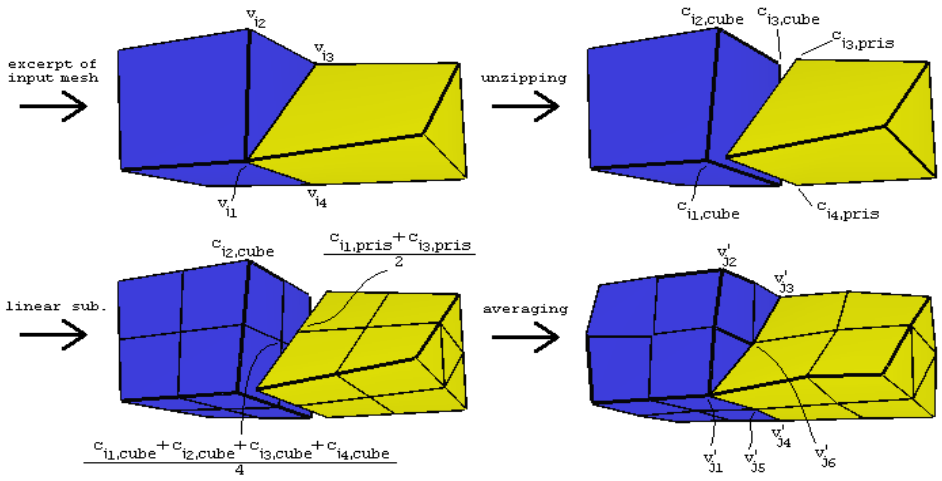

Figure 5.5 : Another example of one round of subdivision inside of a volumetric mesh. An edge-midpoint of a triangular boundary of the prism is topologically identified with the face-midpoint of the adjacent quad of the cube.

from figure 5.1 are considered topologically identical, whenever the vertex indices and the weights of the affine combination are identical. Additionally, whenever a boundary triangle coveres half of a boundary quad, the edge-midpoint inserted by the triangle along the diagonal of the quad is topologically identified with the inserted face-midpoint of the quad. The latter case occurs in figure 5.5.

The averaging pass operates on the mesh after linear subdivision. The characteristic matrices for tetrahedra and octahedra are taken from [SW04] as

$$\Xi_{tetr} = \frac{1}{48}\begin{pmatrix} -3 & 17 & 17 & 17 \\ 17 & -3 & 17 & 17 \\ 17 & 17 & -3 & 17 \\ 17 & 17 & 17 & -3 \end{pmatrix} \quad \text{and} \quad \Xi_{octa} = \frac{1}{24}\begin{pmatrix} 9 & 2 & 2 & 7 & 2 & 2 \\ 2 & 9 & 2 & 2 & 7 & 2 \\ 2 & 2 & 9 & 2 & 2 & 7 \\ 7 & 2 & 2 & 9 & 2 & 2 \\ 2 & 7 & 2 & 2 & 9 & 2 \\ 2 & 2 & 7 & 2 & 2 & 9 \end{pmatrix}.$$

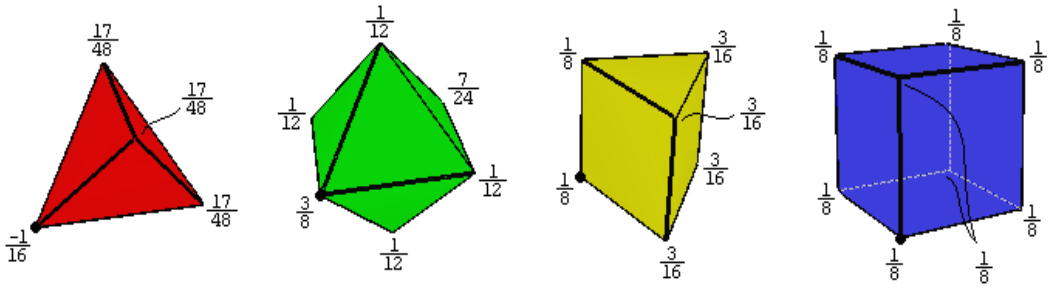

Figure 5.6 : Effect of the characteristic matrix on a single vertex.

For triangular prisms we define

$$\Xi_{pris} = \frac{1}{16}\begin{pmatrix} 2 & 3 & 3 & 2 & 3 & 3 \\ 3 & 2 & 3 & 3 & 2 & 3 \\ 3 & 3 & 2 & 3 & 3 & 2 \\ 2 & 3 & 3 & 2 & 3 & 3 \\ 3 & 2 & 3 & 3 & 2 & 3 \\ 3 & 3 & 2 & 3 & 3 & 2 \end{pmatrix},$$

and Ξ_{cube} is an 8×8 matrix where all entries equal $\frac{1}{8}$. For each shape we gather the vertices of the shape w_{j_k} for $k = 1...n$ in a matrix and multiply the concatenation by the characteristic matrix of the shape. $n = 4$ for tetrahedra, $n = 6$ for octahedra and triangular prisms and $n = 8$ for each cube in the mesh.

$$[w_{j_1} \mid w_{j_2} \mid ... \mid w_{j_n}]\Xi = [w'_{j_1} \mid w'_{j_2} \mid ... \mid w'_{j_n}]. \tag{5.3.1}$$

From the result we extract new vertex positions of the shape: w'_{j_1} replaces w_{j_1}, w'_{j_2} replaces w_{j_2}, etc. Note that in the concatenation the vertex ordering is relevant for octahedra or triangular prisms, due to the shape of Ξ_{octa} and Ξ_{pris}.

Until now, the topological identification of the vertices is not modified under the averaging pass. In a final loop, topologically identical vertices are collapsed into one

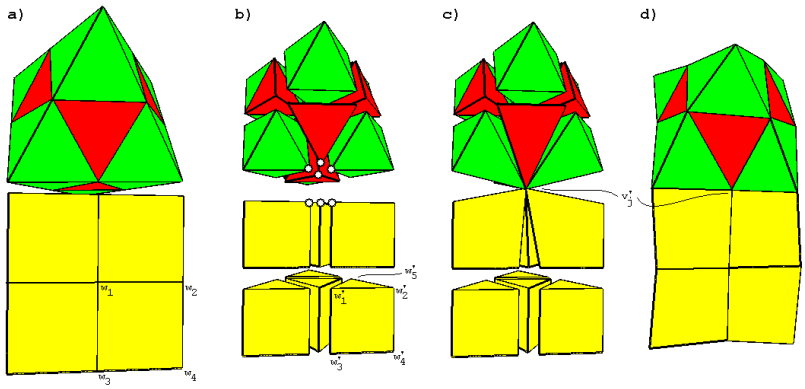

Figure 5.7 : Region of a volumetric mesh is displayed after unzipping and linear subdivision in a). Result of multiplying each shape's vertices with the respective characteristic matrix is shown in b). Vertex positions are chosen for illustration purposes (not obtained by exact evaluation). The vertices of the bottom right prism are enumerated before and after multiplied by Ξ_{pris}. Also, a group of topologically identical vertices is highlighted. c) shows the vertex collapse according to equation 5.3.2 for only one vertex, whereas d) shows the collapse for all vertices.

vertex v'_j of the output mesh. The formula is

$$v'_j = \frac{\frac{1}{14}\sum^{\mu_{toc}} w'_{toc}(j) + \frac{1}{12}\sum^{\mu_{pris}} w'_{pris}(j) + \frac{1}{8}\sum^{\mu_{cube}} w'_{cube}(j)}{\frac{\mu_{toc}}{14} + \frac{\mu_{pris}}{12} + \frac{\mu_{cube}}{8}}, \tag{5.3.2}$$

in which the term $\sum^{\mu_{toc}} w'_{toc}(j)$ denotes the sum over all vertices that are topologically identified with the j-th vertex and belong to tetrahedra or octahedra. μ_{toc} denotes the number of such vertices. The analog holds for $\sum^{\mu_{pris}} w'_{pris}(j)$ and $\sum^{\mu_{cube}} w'_{cube}(j)$.

Then, one round of subdivision is complete. The following example emphasizes the vertex collapse through the averaging pass, easier to visualize in 2D.

Example 5.2. The triangular-quad scheme of [SW03] is briefly presented here. The interested reader may also consult [WS04]. The input to the algorithm is an unstructured mesh consisting of triangles and quads such as in figure 5.8.a. The unzipping

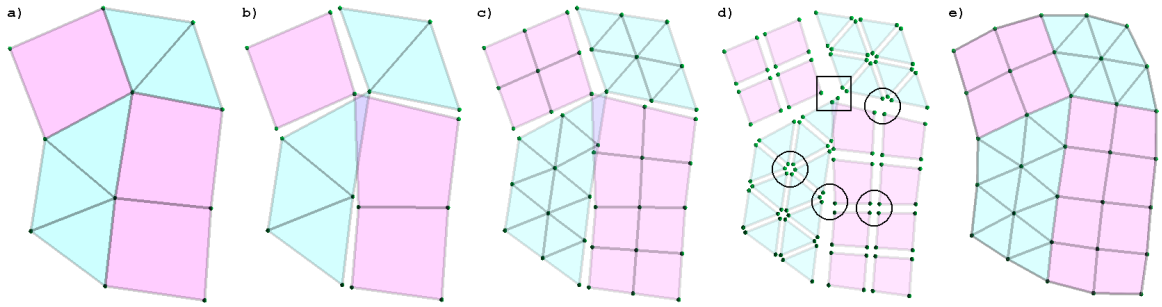

Figure 5.8 : One round of triangular-quad subdivision shown on an exemplary mixed mesh. Example 5.2 explains the process. Vertex positions are chosen for illustration purposes (not obtained by exact evaluation).

procedure clones each vertex as $v_i \longrightarrow \{c_{i,tri}, c_{i,quad}\}$ according to the formula

$$\begin{aligned} c_{i,tri} &= v_i + \delta_i \\ c_{i,quad} &= v_i - \delta_i. \end{aligned} \tag{5.3.3}$$

Heterogeneous touching boundary pairs are now edges that are shared by a triangle and a quad. The distortion at the i-th vertex is

$$\delta_i = \frac{1}{n}\sum_{k=1}^{n}[v_i \mid v_{p_k}] \begin{pmatrix} -\frac{1}{24} \\ \frac{1}{24} \end{pmatrix} = -\frac{1}{24}v_i + \frac{1}{24n}\sum_{k=1}^{n} v_{p_k},$$

when there are n such edges (v_i, v_{p_k}), for $k = 1...n$, adjacent to the i-th vertex. In figure 5.8.b triangles are connected to clones of type tri, whereas the corners of the quads are clones of type $quad$.

Linear subdivision introduces edge- and face-midpoints and redefines the topology, as shown in figure 5.8.c. The averaging pass loops over the new shapes generated by linear subdivision. The characteristic matrix for triangles is

$$\Xi_{tri} = \frac{1}{8}\begin{pmatrix} 2 & 3 & 3 \\ 3 & 2 & 3 \\ 3 & 3 & 2 \end{pmatrix},$$

whereas Ξ_{quad} is a 4×4 matrix with all entries equal to $\frac{1}{4}$. The vertices of each shape are gathered in a matrix with n columns and multiplied by the corresponding Ξ as in

$$[w_{j_1} \mid w_{j_2} \mid ... \mid w_{j_n}]\Xi = [w'_{j_1} \mid w'_{j_2} \mid ... \mid w'_{j_n}].$$

$n = 3$ for triangles and $n = 4$ for quads. w'_{j_1} replaces w_{j_1}, etc. In figure 5.8.d the new positions of the vertices are drawn close to their original positions to indicate several topologically identical vertices surrounded by dark frames.

The linear combination to perform the collapse of topologically identical vertices similar to expression 5.3.2 is

$$v'_j = \frac{\frac{1}{6}\sum^{\mu_{tri}} w'_{tri}(j) + \frac{1}{4}\sum^{\mu_{quad}} w'_{quad}(j)}{\frac{\mu_{tri}}{6} + \frac{\mu_{quad}}{4}},$$

in which the term $\sum^{\mu_{tri}} w'_{tri}(j)$ denotes the sum over all vertices that are topologically identified with the j-th vertex and belong to triangles. μ_{tri} denotes the number of such vertices. The analog holds for $\sum^{\mu_{quad}} w'_{quad}(j)$. In the example mesh the vertices contained by the square are topologically identical and $\mu_{tri} = 3$ and $\mu_{quad} = 2$.

The mesh in figure 5.8.e is the output of the algorithm, ready to perform another round of subdivision.

5.4 Implementation

An open source implementation of the scheme in C_{++} together with a volumetric subdivision utility is available at

`www.hakenberg.de/subdiv/volume.htm`

The program is able to parse mesh files in text format and subdivide a mesh as specified by a user. The outcome is also stored in text format.

5.5 Deformations

Three-dimensional modelling and animation software usually incorporates deformation tools, which allow an artist to vary for instance the pose of a humanoid model, such as raising an arm or bending a knee. Formally, a deformation determines new positions for all model vertices V_m. Often the number of model vertices is large, but the desired deformation is simple, e.g. the distances between nearby model vertices before and after the deformation varies little.

A common approach to reduce the effort in generating deformations is to introduce a few control vertices V_c that belong to a volumetric mesh, which encloses the region of the model that is to be deformed. The numbers in the spoon example in figure 1.2 are $|V_m| = 1852$ whereas $|V_c| = 50$. The vertex positions of the deformed model $\tilde{V}_m$ are defined via matrix multiplication

$$(V_c + H)D = \tilde{V}_m, \tag{5.5.1}$$

where $V_\#$ functions as a $3 \times |V_\#|$ matrix that is a concatenation of the vertex positions. If the matrix of control point excursion $H \in \mathbb{R}^{3\times|V_c|}$ is zero, the identity $V_c D = V_m$ holds. The topology of the model, such as the triangulation, is invariant under deformation.

The rectangular matrix $D \in \mathbb{R}^{|V_c|\times|V_m|}$ is of the form $D = SB$, where the matrix $S \in \mathbb{R}^{|V_c|\times|V_s|}$ takes the control vertices V_c to the k-times subdivided volumetric mesh with vertices V_s as in

$$V_c S = V_s.$$

Let S contain the subdivision weights.

The entries of the i-th column of the matrix $B \in \mathbb{R}^{|V_s|\times|V_m|}$ are the barycentric coordinates of the model vertex $v_i \in V_m$ with respect to the vertices of the (tiny) volumetric shape of the subdivided mesh that contains v_i (in the geometrical sense). All other vertices from V_s, not belonging to the volumetric shape, correspond to a

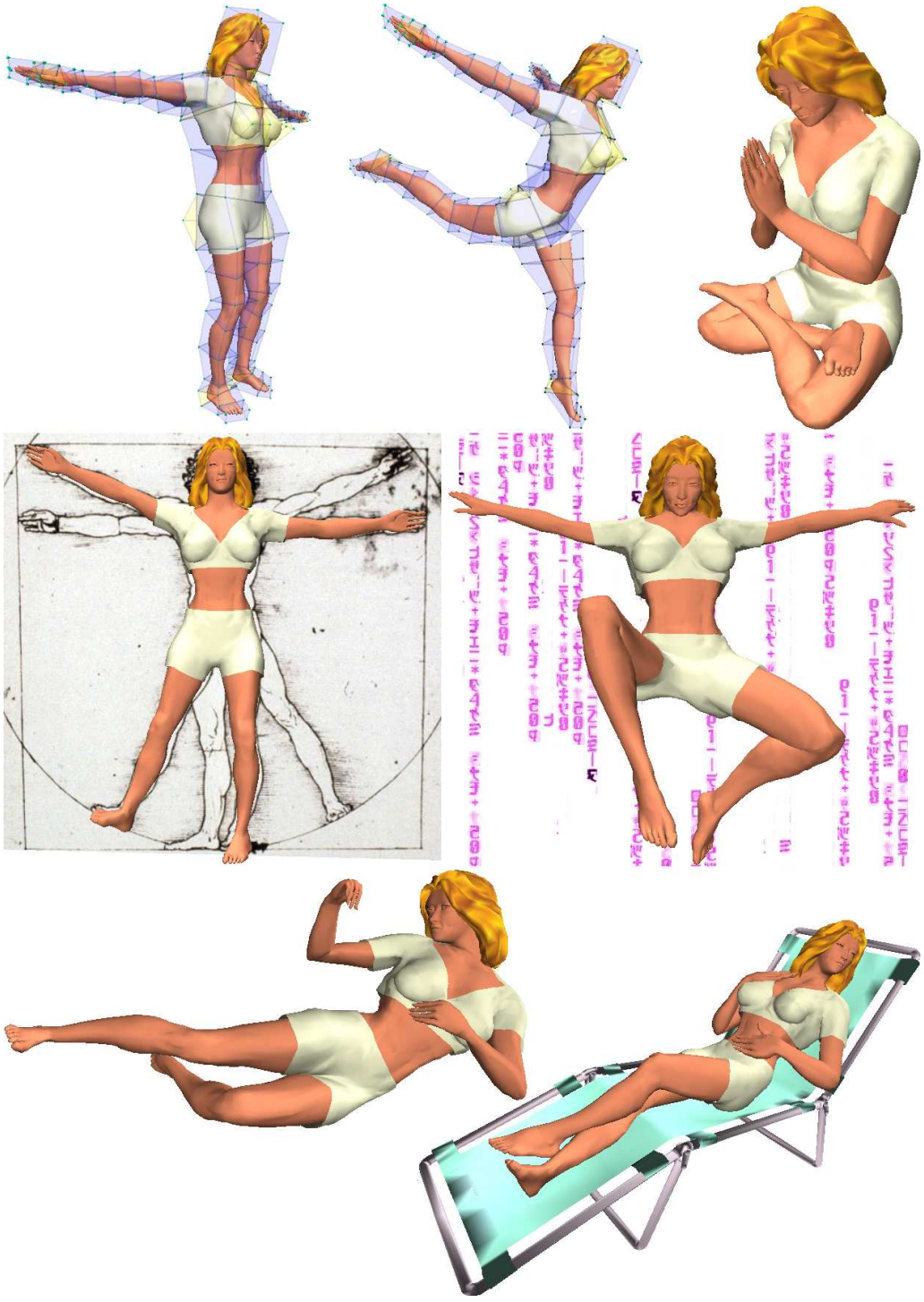

Figure 5.9 : The model *Noma* courtesy of Mike Beals top left is deformed into several poses.

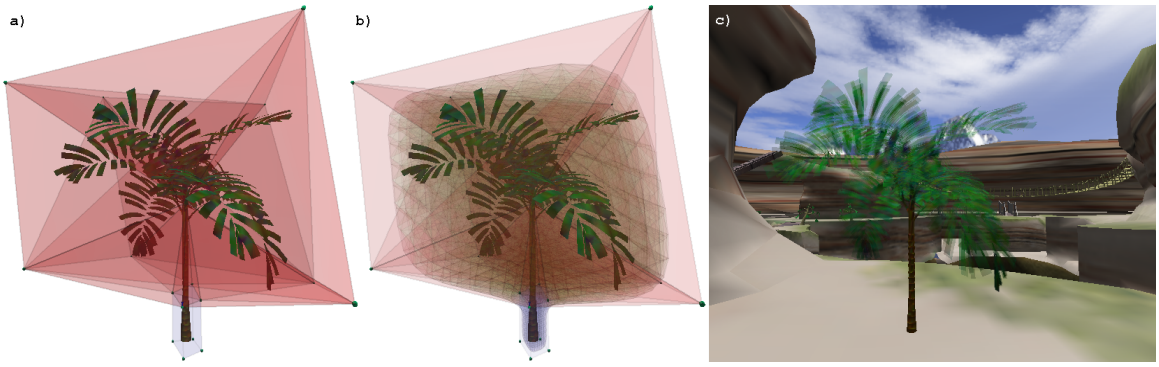

Figure 5.10 : Deformation via a volumetric control mesh a) animates palm in real-time c). The precomputation of matrix D in eq. 5.5.1 involves subdividing the control mesh several times as displayed in b).

zero entry in the i-th column of B. We write

$$V_s B = V_m.$$

The paper [WS02] describes how barycentric coordinates are determined inside convex polytopes, such as for a point enclosed in an octahedron with respect to the six vertices of the octahedron. The boundary of a prism or a cube is patched at least partially by quads, which might not be geometrically planar. In such a case the quads of the shape are triangulated so that the shape is convex, which is possible as long as the shape is not degenerate. Through this process a vertex of the model might be contained by multiple volumetric shapes, in which case we could average the barycentric coordinate contributions.

The deformation results are visually appealing when the depth k of subdivision of the volumetric control mesh is adjusted so that each tiny volumetric shape contains only a few model vertices.

Since deformation of a model is described by a (sparse) matrix multiplication in equation 5.5.1, the computation can be carried out very efficiently. Figure 5.10 illustrates how in a computer game this technique is used to simulate the bending

of a palm tree in the wind. Because the computation is done for each frame of the display instead of being precomputed, the control vertices V_c also make the tree react upon collisions. Edges of the control mesh are treated as springs that in principle force the plant to its originial position .

To achieve the various poses of the humanoid model in figure 5.9, repositioning the $|V_c| = 204$ control vertices individually is too arduous. Instead, we associate a rigid skeleton to the model, which is to approximate the natural skeleton of a human. Joints of the artificial skeleton are located at the knees, shoulders, etc. Then, it makes sense to fix the position of a control point relative to the coordinate system of a nearby joint, so that upon rotating the joints the control points reposition in world coordinates. In the example the number of joints used is 31.

A few control points might need to be positioned manually to compensate for changes in volume that might manifest in the model in the neighborhood of an excessive joint rotation. We experimented with several approaches to automate the correction process but did not find a satisfactory universal solution.

Bibliography

[BS02] C. Bajaj, S. Schaefer, J. Warren, G. Xu: *A subdivision scheme for hexahedral meshes*, The visual computer, Vol. 18, 2002, pp. 409–420

[CC78] E. Catmull, J. Clark: *Recursively generated B-spline surfaces on arbitrary topological meshes*, Computer Aided Design 16(6), pp. 350–355, 1978

[CD02] Y. Chang, K. McDonnell, H. Qin: *A New Solid Subdivision Scheme based on Box Splines*, Proceedings of the seventh ACM symposium on Solid modeling and applications, ACM Press, pp. 226–233, 2002

[CQ03] Y. Chang, H. Qin: *A framework for Multi-dimensional Adaptive Subdivision Objects*, Proceedings of Solid Modeling and Applications, To appear, 2004

[DS78] D. Doo, M. Sabin: *Behaviour of recursive division surfaces near extraordinary points*, Computer Aided Design 10(6), pp. 356–360, 1978

[CJ96] R. MacCracken, K. Joy: *Free-Form Deformations With Lattices of Arbitrary Topology*, SIGGRAPH Computer Graphics Proceedings, pp. 181–188, 1996

[Le03] A. Levin: *Polynomial generation and Quasi-interpolation in stationary non-uniform subdivision*, Computed Aided Geometric Design 20(1), pp. 41-60, 2003

[$L^2$03] A. Levin, D. Levin: *Analysis of Quasi-Uniform Subdivision*, Applied and Computational Harmonic Analysis 15(1), pp. 18–32, 2003

[Lo87] C. Loop: *Smooth subdivision surfaces based on triangles*, Master's thesis, Department of Mathematics, University of Utah, 1987

[MW01] G. Morin, J. Warren, H. Weimer: *A subdivision scheme for surfaces of revolution*, Computer-Aided Geometric Design 18, pp. 483–502, 2001

[Re95] U. Reif: *A unified approach to subdivision algorithms near extraordinary points*, Computer-Aided Geometric Design 12, pp. 153–174, 1995

[SW04] S. Schaefer, J. Warren, J. Hakenberg: *Smooth Subdivision of Tetrahedral Meshes*, Eurographics Symposium on Geometry Processing, pp. 151–158, 2004

[SW03] S. Schaefer, J. Warren: *On C^2 Triangle/Quad Subdivision*, to appear in ACM Transactions on Graphics, 2003

[St01] J. Stam: *On subdivision schemes generalizing B-spline surfaces of arbitrary degree*, Computer-Aided Geometric Design 18, pp. 383–396, 2001

[WS02] J. Warren, S. Schaefer, A. Hirani, M. Desbrun: *Barycentric coordinates for convex sets*, Rice University technical report

[WS04] J. Warren, S. Schaefer: *A Factored Approach to Subdivision Surfaces* IEEE Computer Graphics, pp. 74–81, May/June 2004

[WW03] J. Warren, H. Weimer: *Subdivision Methods for Geometric Design*, Morgan Kaufmann, 2003

[ZS01] D. Zorin, P. Schroeder: *A unified framework for primal/dual quadrilateral subdivision schemes*, Computer-Aided Geometric Design 18, pp. 429–454, 2001

[ZL04] A. Zulti, A. Levin, D. Levin, M. Taicher: *C^2 subdivision over triangulations with one extraordinary point*, 2004